ELSEVIER

Contents lists available at ScienceDirect

Journal of Hydrology

journal homepage: www.elsevier.com/locate/jhydrol



Research papers

Contrasting storage-flux-age interactions revealed by catchment intercomparison using a tracer-aided runoff model



T. Piovano^a, D. Tetzlaff^{b,c}, M. Maneta^d, J.M. Buttle^e, S.K. Carey^f, H. Laudon^g, J. McNamara^h, C. Soulsby^{a,c,*}

- ^a Northern Rivers Institute, University of Aberdeen, Aberdeen AB24 3UF, UK
- ^b Geography Department, Humboldt-Universität zu Berlin, 12489 Berlin, Germany
- c IGB Leibniz-Institute of Freshwater Ecology and Inland Fisheries. 12587 Berlin, Germany
- ^d Geosciences Department, University of Montana, Missoula, MT 59812, Montana, Unites States
- ^e Department of Geography, Trent University, Peterborough K9L 0G2, Ontario, Canada
- f School of Geography and Earth Sciences, McMaster University, Hamilton L8S 4K1, Ontario, Canada
- g Swedish University of Agricultural Sciences, Department of Forest Ecology and Management, 907 36 Umeå, Sweden
- h Department of Geosciences, Boise State University, Boise, ID 83725, USA

ARTICLE INFO

This manuscript was handled by Marco borga, Editor-in-Chief, with the assistance of Sally Thompson, Associate Editor

Keywords: Storage Water ages Storage-discharge Hydroclimatic forces Phase-space Non-linearity

ABSTRACT

Water storage dynamics modulate fluxes within catchments, control the rainfall-runoff response and regulate the velocity of water particles through mixing associated processes. Tracer-aided models are useful tools for tracking the interactions between catchment storage and fluxes, as they can capture both the celerity of the runoff response and the velocity of water particles revealed by tracer dynamics. The phase-space reconstruction of modelled systems can help in this regard; it traces the evolution of a dynamic system from a known initial state as phase trajectories in response to inputs. In this study, we compared the modelled storage-flux dynamics obtained from the application of a spatially distributed tracer-aided hydrological model (STARR) in five contrasting long-term research catchments with varying degrees of snow influence. The models were calibrated using a consistent multivariate methodology based on discharge, isotope composition and snowpack water equivalent. Analysis of extracted modelled storage dynamics gave insights into the system functioning. Large volumes of total stored water needed to be invoked at most sites to reconcile celerity and travel times to match observe discharge and isotope responses. This is because changes in dynamic storage from water balance considerations are small when compared to volume of storage necessary for observed tracer dampening. In the phase-space diagrams, the rates of storage change gave insights into the relative storage volume and seasonal catchment functioning. The storage increase was dominated by hydroclimatic inputs; thus, it presented a stochastic response. Furthermore, depending on the dominance of snow or rainfall inputs, catchments had different seasonal responses in storage dynamics. Decreases in storage were more predictable and reflected the efficiency of catchment drainage, yet at lower storages the influence of ET was also evident. Activation of flow paths due to overland and near-surface flows resulted in non-linearity of catchment functioning largely at high storage states. The storage-discharge relationships generally showed a non-linear distribution, with more scattered states during wettest condition. In turn, all the catchments exhibited an inverse storage effect, with modelled water ages decreasing with increasing storage as lateral flow paths were activated. Insights from this inter-comparison of storage-flux-age dynamics show the benefits of tracer-aided hydrological models in exploring their interactions at well-instrumented sites to better understand hydrological functioning of contrasting catchments.

1. Introduction

The hydrological function of catchment systems integrates complex physical processes across a range of temporal and spatial scales giving rise to typically non-linear rainfall-runoff responses (e.g. Tsonis et al.,

1993; Jayawardena and Lai, 1994; Koutsoyiannis and Pachakis, 1996; Sivakumar et al., 2009 and review by Sivakumar, 2000). This complexity has been simplified through the exploration of storage-discharge dynamics, which provides a useful way of understanding how climatic forcing, antecedent conditions and catchment characteristics interact to

E-mail address: c.soulsby@abdn.ac.uk (C. Soulsby).

^{*} Corresponding author.

T. Piovano, et al. Journal of Hydrology 590 (2020) 125226

produce rather consistent rainfall-runoff responses (Kirchner, 2009). Such dynamics also provide a powerful basis for inter-catchment comparison, though this is largely unrealised (McNamara et al., 2011). Still, the nature of catchment storage-discharge interactions is complex and difficult to quantify by direct observation. Hydroclimatic dynamics, which represent the input to catchment systems, are intrinsically stochastic and non-linear, often exhibiting marked seasonality as well as interannual variability (e.g. Rodriguez-Iturbe and De Power, 1989; Sharifi et al., 1990; Houghton, 1991; Lorenz, 1991; Georgakakos et al., 1995; Puente and Obregn, 1996; Sivakumar et al., 1999). Furthermore, many hydrologic processes that depend on catchment attributes (e.g. geology, topography, soils, land use, etc.) and on the initial catchment conditions (i.e. initial wetness) contribute to the non-linearity in the rainfall-runoff transformation and may cause hysteresis in the storagedischarge relationship. In addition, catchment size determines the relative influence of hillslope flow processes and routing through channel networks in determining the timing of the hydrological response (Robinson et al., 1995). Characterising all these factors is challenging and physically quantifying storage is difficult though geophysical and remote sensing methods are proving increasingly useful (Rodell et al., 2009; Soulsby et al., 2016). Given these uncertainties, various hydrological models have recently been highlighted as tools to explore the non-linearities of storage-discharge interactions in complex catchments (Beven and Davies, 2015; Harman, 2015; Soulsby et al., 2015).

In order to be used to explore catchment dynamics, it is fundamental that hydrological models correctly represent the non-linearities of the catchment rainfall-runoff response. Traditionally, estimating storage dynamics in models has been a means to understanding how antecedent conditions regulate the volume and celerity (i.e. how fast perturbations are transmitted through the flow domain) of the runoff response (Dooge, 1967). This has usually been based on calibration to runoff responses alone. Increasingly, however, it is recognised that the "dynamic" storage needed to produce observed catchment responses is much less than the "total" storage that controls the velocity of water particles and often produce surprisingly long catchment travel times (Soulsby et al., 2011; Staudinger et al., 2017). Insights from conservative tracers, such as stable isotopes, have shown that larger volumes of stored water need to be invoked to produce the mixing needed to damp and lag the dynamics of the rainfall-runoff transformation of conservative tracers (Kirchner et al., 2000; Birkel et al., 2011). Thus, if hydrological models are able to capture both input-output transformations of rainfall-runoff and conservative tracers, they can characterise the celerity of the runoff response, as well as providing estimates of the velocity of water particles and associated ages (Weiler et al., 2003; McDonnell and Beven, 2014). This capacity of hydrologic models allows the interactions between catchment storage, flux and age dynamics to be explored (Birkel and Soulsby, 2015) and can help explain how catchments respond to rainfall or snowmelt events in a matter of minutes and hours, but release water that has been stored for many months or years (Kirchner, 2003).

Models can also help distinguish the non-linearities in catchment responses that are due to variable forcing inputs and those related to intrinsic catchment conditions. In models, inputs are controllable, each internal variable can be individually "observed", and the sensitivity of the response to external inputs and internal model states can be assessed. An additional advantage of using models is that they permit us to track individual solutions corresponding to specified forcing inputs and initial conditions. Therefore an ensemble of model runs simulating a large range of forcing inputs and initial conditions can be used to reconstruct an approximation of the phase portrait that reveals all feasible solutions and states of a catchment (i.e. total water storage), the rate at which changes in storage occur and an indication of the model uncertainty. This shape of the phase portrait can be interpreted in terms of the behaviour of the dynamic system (Maneta et al., 2018). The region of these trajectories and the visualisation of potential system attractors can give qualitative insights into the complexity, dynamic

stability and non-linearity of the system. Although approaches for analysing hydrological systems on the phase-space reconstruction using streamflow time-series have been investigated in the past (e.g. Jayawardena and Lai, 1994; Porporato and Ridolfi, 2003; Sivakumar et al., 2007; Sivakumar and Singh, 2012), relatively few applications have used modelled storages, especially using tracers as additional constraints (Duffy, 1996; Brandes et al., 1998; Beven and Davies, 2015).

Although models portray virtual environments, they can help us understand the dynamics of real systems, and provide a standardised tool for inter-comparison of the hydrological functioning of catchments with contrasting landscape characteristics and different hydroclimatic regimes (Beven and Davies, 2015). Recent advances in tracer aided modelling have elucidated some of these dynamics, in terms of celerity of response and particle velocities, in contrasting geographical environments and hydroclimatic settings (e.g. Hrachowitz et al., 2013; Birkel et al., 2015; Peralta-Tapia et al., 2016; Sprenger et al., 2018b). In these types of models, the inclusion of conservative tracers can help to better constrain the model and obtain a more plausible response. Although calibration based solely on the hydrograph remains the most common practice in hydrological modelling, several studies showed how models that combine tracers and hydrology can increase understanding of internal catchment processes (Beven, 1993; Kirchner, 2006; Rinaldo et al., 2011). These analyses have used a full range of modelling approaches from lumped models (Iorgulescu et al., 2005; Stadnyk et al., 2005; Dunn et al., 2008; Fenicia et al., 2008a,b; Birkel et al., 2016), to semi-distributed conceptual models (Uhlenbrook et al., 2004; Stadnyk et al., 2013; van Huijgevoort et al., 2016a; Delavau et al., 2017) and more physically-based models (Kuppel et al., 2018; Smith et al., 2019). The range of catchment conditions considered vary from those with high storage (> 1000 mm), long travel times (> 5 years) and attenuated hydrological response, to others with low storage (< 200 mm), short travel times (< 0.5 years) and closer coupling between celerity and water travel times (Hrachowitz et al., 2010). The interaction between catchment characteristics and climate affect storage-flux-age interactions (Ala-aho et al., 2017b). This is particularly evident in terms of high precipitation inputs which drive shorter travel times (e.g. Dehaspe et al., 2018; Zhang et al., 2019), or low precipitation inputs and high evapotranspiration rates that drive longer travel times (Douinot et al., 2019).

The motivation behind this study was to use tracer-aided models as a basis for comparing the storage - flux - age interactions of contrasting experimental catchments. Crucially, the tracer-aided nature of the modelling gives much more realistic characterisation of the catchment storage activated in tracer damping, which in turn determines the velocity of water particles and the resulting ages of catchment storage compartments and associated fluxes. We used the Spatially distributed Tracer-Aided Rainfall-Runoff (STARR) model across a range of northern/montane catchments. Such catchments tend to be under-studied compared to the temperate region and have an additional complexity which relates to varying characteristics of snowpack influence and melt, and the different degree of snowmelt influence on storage dynamics and runoff (Tetzlaff et al. 2015a). Many such catchments are also experiencing rapid climatic warming which will change flux storage dynamics, with widespread implications for water management (Tetzlaff et al., 2015b). Specifically, we compare standardised STARR simulations for these catchments for an inter-comparison of to examine how storage changes relate to the dominant input and output fluxes and associated water ages across multiple years of simulation. STARR was originally developed for an upland catchment in Scotland (van Huijgevoort et al., 2016a), and subsequently adapted to capture the influence of snowmelt processes (Ala-aho et al., 2017a) and frozen ground (Piovano et al., 2019) on hydrological and isotope dynamics. The model has been successfully applied to a range of catchments (e.g. Ala-aho et al., 2017b; Dehaspe et al., 2018). Whilst there are obvious limitations in using modelled, rather than observed, systems behaviour, the common approach used here provides a means for a unique

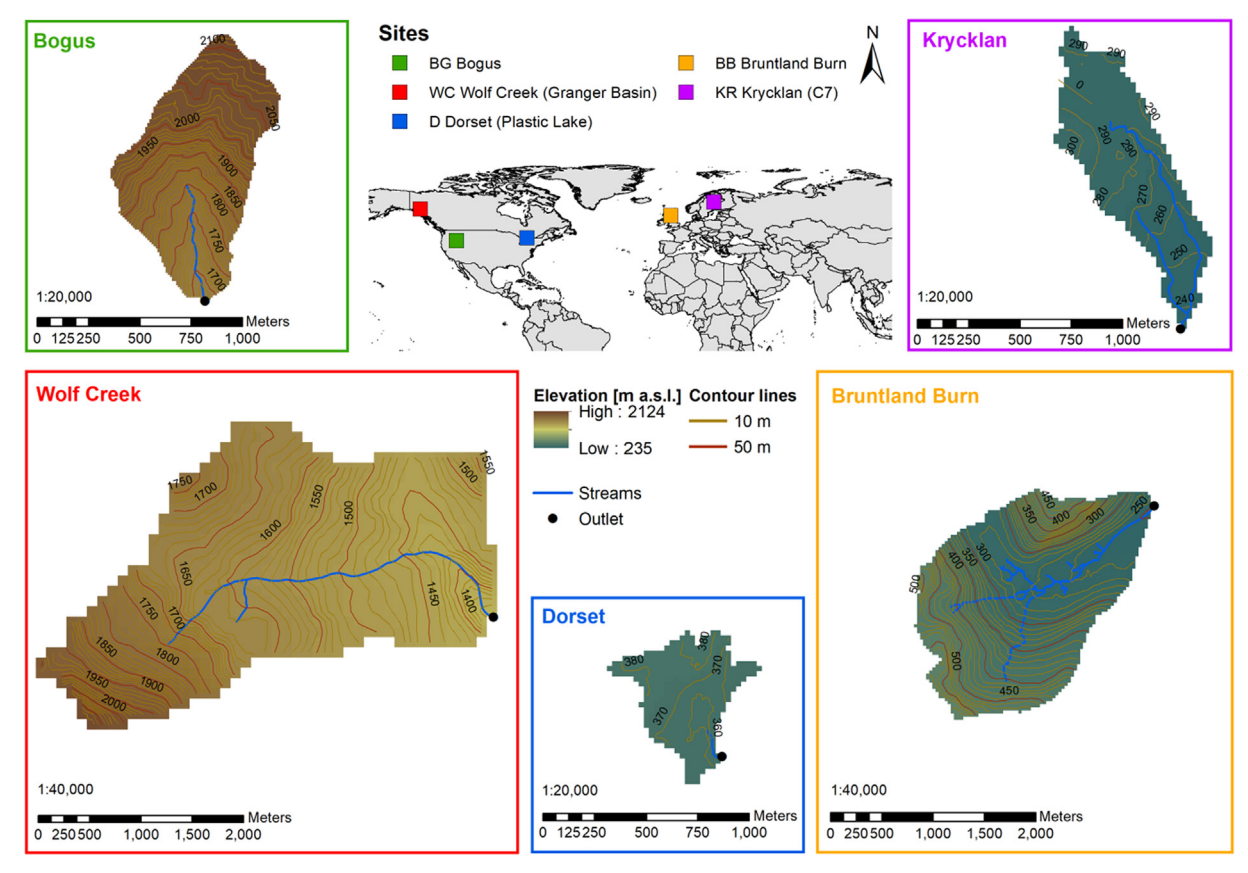


Fig. 1. Maps of the modelled catchments: Bogus (BG), Wolf Creek (WC), Dorset (D) Brundtland Burn (BB) and Krycklan (KR). Note different scales for the larger WC and BB sites compared with the others.

catchment inter-comparison when direct observations are unavailable (Beven and Davies, 2015). The specific objectives of the study are to: (1) use a tracer-aided semi-distributed rainfall-runoff-model as a common framework for comparing storage dynamics in contrasting catchments; (2) identify how hydroclimatic forcing and catchment characteristics interact to produce stochastic/deterministic and linear/nonlinear behaviours by examining the storage dynamics in phase-space diagrams; and (3) identify inter-catchment differences in how storage dynamics control runoff generation and mixing interactions which determine the age of stream water.

2. Data & methods

2.1. Study sites

Five catchments encompassing a range of geological, topographic and hydroclimate characteristics across northern latitudes were included in the study (Fig. 1): Bogus Creek (BG), part of the Dry Creek experimental watershed (DCEW) in Idaho (USA); Bruntland Burn (BB) in Scotland; Plastic Lake in the Dorset (D) watersheds in Ontario (Canada); sub-catchment C7 of the Krycklan Research Catchment (KR) in Sweden; and Granger Basin, a sub-catchment of Wolf Creek (WC) in the Yukon Territory (Canada). All the study sites are established, long-term experimental catchments, details of which are available elsewhere (e.g. Tetzlaff et al., 2015a,b).

The study catchments range in size from $0.23~\rm km^2$ at D to $7.8~\rm km^2$ at WC, with BG and KR also having smaller areas ($<1~\rm km^2$), but BB being larger ($3.2~\rm km^2$). The catchments, except for BB, have a strong snowmelt influence in their hydrological response, with at least 25% of precipitation falling as snow (Table 1), and span a relatively wide range of climatic conditions. WC has the coldest and driest conditions typical of a subarctic climate. Hydrographs at WC are therefore highest during

snowmelt and usually peak in May, while low flows occur under-ice between autumn and late spring (Fig. 2). Conversely, BB shows the wettest conditions with all monthly average temperatures above 0 °C. Seasonality of evapotranspiration at BB gives rise to lower summer flows and discharge peaks between November and February, however high flows can occur throughout the year. BG and KR have similar cumulative precipitation over the year with around half falling as snow at KR (Laudon and Löfvenius, 2016) and more than 50% at BG. Average temperatures at BG are higher than at KR, but both catchments have sub-zero monthly mean temperature between November and March. The hydrologic response is also different: at BG snowmelt dominates the hydrograph from March to June typically peaking in May, while low flows occur during the rest of the year. Snowmelt at KR peaks in April-May, though high flows of similar magnitude can occur in response to summer rainfall, while flows are lower in the cold winter. D has a humid continental climate, with sub-zero monthly mean temperatures from December to March. The hydrograph peaks occur usually during snowmelt, with rainfall-generated summer peaks and occasional cessation of flow during summer droughts.

Topography and geology also exert strong controls on the hydrological behaviour of the study sites. BG presents a V-shaped fluvial valley with the highest elevations across all sites. It is characterized by fractured granodiorite, covered by a thin layer (< 1 m) of permeable sands (McNamara et al., 2005). Conversely, WC has a similar elevation range to BG but limited capacity for water storage due to extensive discontinuous permafrost (around 70% of the area) that acts in a similar way to impermeable bedrock (Piovano et al., 2019). The deeper geology of WC is sedimentary, overlain by a mantle of glacial till. The BB, D and KR sites have similar combinations of riparian peatlands overlying drift deposits (Dillon and LaZerte, 1992; Laudon et al., 2013; Tetzlaff et al., 2014). However, BB has much steeper topography compared to the flat KR and the gently sloping D catchments. At BB,

Table 1
Site characteristics: area [km²], average annual temperature T [°C], average annual P [mm], percentage of precipitation falling as snow, Latitude, Longitude, minimum and maximum elevation [m a.s.l.], total simulation period and the length in year of spin-up period.

	Area [km2]	T [°C]	P [mm]	% of P as Snow	Latitude	Longitude	Min elev. [m a.s.l.]	Max elev. [m a.s.l.]	Simulation period	Spin-up length [year]
BG	0.6	8.8	1330	> 50	43°42′N	116°10′E	1684	2135	2007-2014	2
BB	3.2	7	670	< 5	57°8′N	3°20′E	250	530	2011-2016	1
D	0.23	5	1050	> 25	45°11′N	78°50′W	351	385	2010-2016	2
KR	0.5	2.4	680	35-50	64°14′N	10°46′E	235	306	2004-2012	1
WC	7.8	-0.1	260	40	60°32′N	135°11′W	1310	2080	2014-2016	2

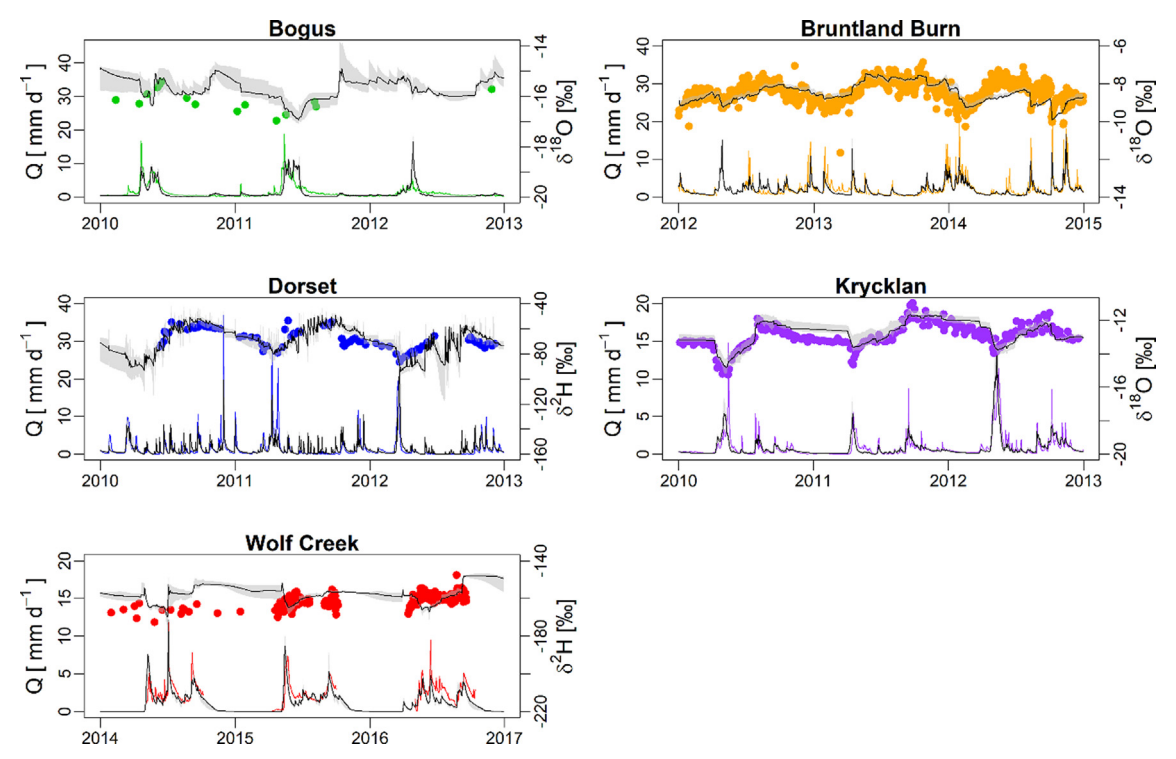


Fig. 2. Three year streamflow hydrographs (lines) and stream isotope signatures (dots) in the study catchments. Also shown are the STARR simulations of daily discharge and stream isotopes (grey envelopes). Note different Y scales.

steep hillslopes are covered by podzolic soils and the wide, glaciated valley bottoms are covered by organic soils capable of generating overland flow and are underlain by up to 30 m of glacial drift, with significant groundwater storage (Soulsby et al., 2016). At the flatter D and KR basins, the presence of wetlands impact their hydropedological properties: a minerogenic mire covers 18% of KR and a conifer wetland occupies 7–10% of D. In the mire at KR, overland flow takes place during periods of intense rain or snowmelt (Peralta-Tapia et al., 2015b), while subsurface flow paths dominate the rest of the catchment, where podzolic soils are formed above compact basal till. Weakly developed podzols have formed on thin sandy basal tills at D (Kirkwood and Nesbitt, 1991). Leading to thin (~0.5 m) soil cover with bedrock outcrops comprising 10% of the area (Dillon and LaZerte, 1992). The bedrock limits groundwater contributions and the dominant runoff mechanisms is lateral flow at the soil-bedrock interface.

Vegetation across the catchments ranges from forests to *Sphagnum* bogs. In particular, BG is mainly covered by shrubs (*Prunus* spp. and *Ceanothus* spp.), with a small fraction of taller tree canopies (*Pseudotsuga menziesii* and *Pinus ponderosa*) near the stream. At BB, the steep slopes are dominated by heather (*Calluna vulgaris*) with patches of Scots pine (*Pinus sylvestris*) forests, while the valley bottom is covered by *Sphagnum* dominated peatlands. Most of D is forested with white pine (*Pinus strobus*), hemlock (*Tsuga canadensis*) and some red oak, while the wetland area is forested with birch (*Betula* spp.) and black spruce (*Picea mariana*) (Devito et al., 1996). KR is covered by conifer

boreal forest (*Picea abies* and *Pinus sylvestris*), except for the canopy-free minerogenic mire with *Sphangnum* moss. At WC, the vegetation consists predominantly of willow (*Salix*) and birch (*Betula*) shrubs.

2.2. The STARR model

STARR is a spatially explicit hydrological model that simulates water fluxes, storage dynamics, isotope ratios, and water ages (Fig. 3). Originally developed for the BB catchment (van Huijgevoort et al., 2016a,b), it has a structure similar to the HBV-light model (Lindström et al., 1997) and a scheme for tracer tracking and mixing similar to tracer-aided lumped models (Birkel et al., 2011). The original model has been modified by Ala-aho et al. (2017a) to include a snowmelt routine that simulates the isotopic composition of the snowpack and melt water. Further adaptation by Piovano et al. (2019) allows the model to simulate the dynamics of frozen ground. As full details are in these original papers, only a brief summary follows.

STARR is driven by input time series, including precipitation, temperature, relative humidity, solar radiation, wind speed and precipitation isotope composition. A digital elevation model is used to route water downslope. Temperature and precipitation are spatially distributed according to an elevation factor, while radiation terms are adjusted for the influence of slope, aspect and canopy sheltering. The model is usually applied at a daily time step, though more recently subdaily scales have been used (Dehaspe et al., 2018). Water balance

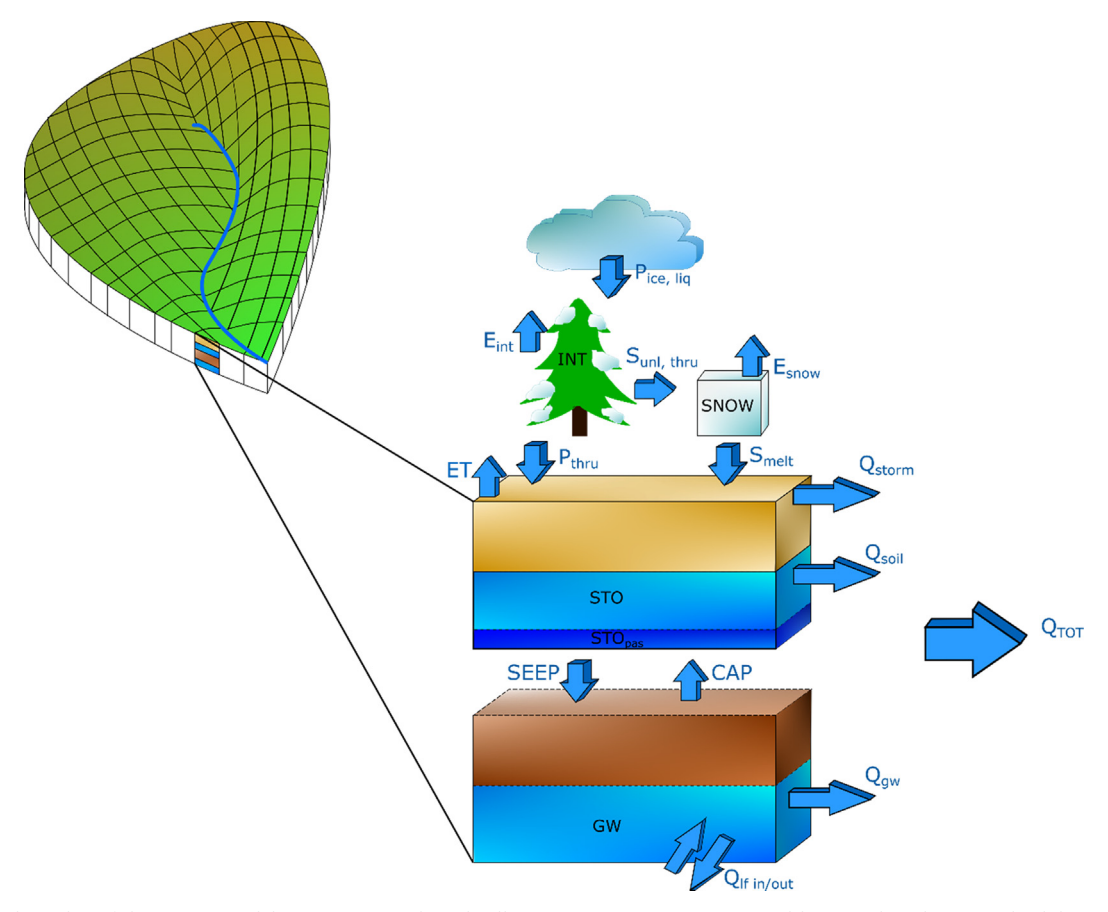


Fig. 3. Conceptual graphic of the STARR model structure at each grid cell. Input precipitation is portioned between liquid (P_{liq}) and solid (P_{ice}); INT is canopy interception module and SNOW the snow module, with: water fraction stored in vegetation (INT), evaporation from vegetation (E_{int}), unloading (S_{unl}), throughfall from snow precipitation bypassing the interception storage (S_{thru}), throughfall from interception (P_{thru}), water stored as snow (SNOW), sublimation from snow (E_{snow}), melting from snow (S_{melt}). STO is the soil storage, with: evaporation from soil (ET), passive storage (STO_{pas}), overland flow (Q_{storm}), contribution to discharge from soil (Qsoil), contribution to groundwater recharge (SEEP). GW is the groundwater storage, contribution to discharge Q_{gw} and lateral in/out flow from/to neighbouring cells (Q_{If} in/out). Q_{TOT} is the total routed discharge.

modelling equations are applied on grid cells, and fluxes from each cell are routed to the neighbouring cell according to the local drainage direction based on topography (Fig. 3). The spatial scale of the grid in the model applications spanned from 10x10 m² to 100x100 m² depending on catchment size (Ala-aho et al., 2017b). For each model routine, water fluxes/storages are estimated according to the mass balance, while isotope ratios are estimated according to mixing equations under the assumption of complete mixing in each cell for each compartment, though this integrates to partial mixing in terms of stream flow generation at the catchment scale. Incoming precipitation is partitioned between liquid (Pliq) or solid (Pice) precipitation according to calibrated temperature thresholds. An interception compartment accounts for the fraction of precipitation intercepted by vegetation (INT), the fraction of throughfall (Pthru) and evaporation from vegetation (Eint). For the snow fraction (SNOW), tree canopy interception (INT) and unloading (Sunl) account for the assumption that interception efficiency decreases with canopy snow load and increases with canopy density, and that snow unloading from vegetation increases with time (Ala-aho et al., 2017a). The snow compartment is energy-based; hence, for each time step an energy balance is solved on net radiation, latent and sensible heat, heat advection from precipitation, and heat storage in the snowpack. Therefore, sublimation (E_{snow}) or melt (S_{melt}) fluxes from snow storage can be simulated. For the isotopes, the energy basis of the snow routine accounts for sublimation fractionation of snow isotope composition both of canopy intercepted snow and the ground-level snowpack water, as well as the isotopic depletion of snowmelt (Ala-aho et al., 2017a).

Effective precipitation (sum of contribution from INT and SNOW

routine) either enters the soil compartment or is routed as direct discharge (Q_{storm}) if the maximum soil storage is exceeded. Water that enters soil storage can either generate discharge (and be routed to the total discharge Q_{TOT} as Q_{soil}), be stored in the soil (STO), evaporate (ET) or contribute to groundwater recharge (SEEP). The storage-discharge relationship in the soil box is modelled as a power law through calibrated parameters (see Ala-aho et al., 2017b for details). The field capacity is modelled as the amount of water that is retained in the soil, defined by parameters for volumetric field capacity and soil depth. This conceptualisation allows a physically based parametrisation and nonlinear seepage and outflow processes with high soil storage values. In addition, the soil module has a passive storage (STO_{pas}) accounting for a fraction of stored water that does not contribute to discharge, but increases the total mixing volume for isotopes. The inclusion of the passive storage conceptualises the storage needed to damp the tracer signal in addition to the dynamic storage needed to generate discharge. In the groundwater routine, a recession parameter (calibrated) regulates the linear contribution to the outflow (Q_{GW}), while it can contribute an upward flux to soil storage (CAP) under a prevailing hydraulic gradient. A lateral flow term ($Q_{lf\ in,out}$) allows the water from a cell to flow to neighbouring cells in the groundwater compartment, according to slope and elevation. Unlike the soil storage that has a limited storage capacity, the groundwater storage (GW) is unconfined.

Parameters regulating the soil sub-routine were subdivided into hillslope and valley bottom cells at BB; and into forest and wetland cells at D and KR (details in Ala-aho et al., 2017b; Piovano et al., 2018). At WC, a similar differentiation has been made – with a subdivision

between properties of the lower and upper basins. However, a critical difference at WC is that the field capacity parameter has been modelled as time-variant, based on the day of the year, in order to include the influence of thaw dynamics (Piovano et al., 2019).

For each routine, water ages are estimated by tracking input fluxes, similar to the tracers. Specifically, when precipitation enters the system it has an age of 1 day. Stored water in the compartments get 1 day older at each daily time step. Through the mixing and water exchanges between model routines and model cells, water ages evolve dynamically in time and space, in a similar way to the water isotope composition.

Commonly, a spin-up period is necessary to initialise the modelled storages and isotope compositions (Table 1). Some of the model parameters are prescribed, while some others (usually around 15) are randomly sampled using a Monte Carlo approach (see van Huijgevoort et al., 2016a,b for details). The performance of the model parameters was evaluated by comparing simulated and observed hydrological and isotopic responses (see calibration details). Each model simulation includes information on storages, fluxes and water age in each model compartment (evaporation, soil storage, etc.) at each time step.

2.3. Model calibration

The data we used in the analysis to compare storage-flux-age dynamics across the study catchments were obtained from earlier calibrated simulations of STARR described in earlier works (Ala-aho et al., 2017b; Piovano et al., 2018, 2019). Fig. 2 shows three years of simulated and observed discharge and isotope composition of streamflow for each of the study catchments. For each site, the model was calibrated using an identical Monte Carlo approach to sample the parameter space. Multi-variate calibration (Ala-aho et al., 2017b) was conducted over the period of available data to select the best performing parameters from 10,000 Monte Carlo runs that match simultaneously observed timeseries of discharge, snow water equivalent (SWE) and best available stream water isotope (δ^{18} O for BB, BG, and KR; δ^{2} H for D and WC). For each simulation, three efficiency metrics were used: Kling-Gupta efficiency (KGE; Gupta et al., 2009) for evaluating discharge and SWE; and mean absolute error (MAE) for evaluating isotope simulations (except for BB, for which the calibration included only discharge and isotopes due to the very limited SWE amounts). The selection of best parameter ensemble was achieved by calculating the empirical cumulative distribution functions of these three efficiency metrics and recording the *n* best simulations that concurrently had the highest values of KGE for discharge and SWE, and the lowest value of MAE for stream water isotopes. In the results presented here, the best five simulations (n = 5) are used to give an indication of model uncertainties induced by alternative parameterizations whilst still allowing differences of individual parameter sets to be observed in the resulting plots. Earlier exploration of the best 10 or 25 simulations showed a similar spread of results, but the density of data points made the phase-space plots difficult to interpret. Hence, 5 was selected as a compromise to show the degree of uncertainty, whilst allowing the trajectories of individual parameter sets to be shown. Details of the calibration are reported in earlier papers: Ala-aho et al. (2017b) for BB, BC, KR; Piovano et al. (2018) for D, Piovano et al. (2019) for WC. Reasonable results for flow, isotopes and SWE allowed cautious inferences about storages - flux interactions to be made and compared across sites (Table 2).

2.4. Data analysis

In order to assess and compare storage-flux-age dynamics for each catchment we considered some of the following STARR model outputs. Specifically, for each catchment we used time series of (a) catchment averaged soil storage (STO) and groundwater storage (GW), (b) discharge (Q) at the outlet cell, (c) streamflow water age (Age) at the outlet cell and (d) catchment evapotranspiration (ET). To conduct the comparative analysis, we aggregated grid cell-scale soil and groundwater

Table 2

Ranges of efficiencies based on the 5 best simulations at the different sites: KGE (Q) of discharge, MAE for isotope composition of streamwater (note the different analysed isotopes: δ^{18} O in the case of BG, BB and KR, while δ^2 H in the case of D and WC), KGE(SWE) of snow water equivalent.

	KGE(Q)	[-]	MAE(isotope)	[‰]	KGE(SWE) [-]	
	Min	Max	Max	Min	Min	Max
BG	0.66	0.74	0.43 (δ ¹⁸ O)	0.27 (δ ¹⁸ O)	0.81	0.83
BB	0.77	0.78	$0.39 \ (\delta^{18}O)$	$0.38 \ (\delta^{18}O)$	_	-
D	0.64	0.69	7.25 (δ^{2} H)	6.88 (δ^2 H)	0.62	0.69
KR	0.69	0.78	$0.46 \ (\delta^{18}O)$	$0.35 (\delta^{18}O)$	0.62	0.66
WC	0.59	0.67	4.94 (δ^2 H)	4.61 (δ^2 H)	0.71	0.72

storage values as well as ET fluxes to produce catchment-averaged time series. Secondly, in order to compare the behaviour of modelled storage between the catchments, we took into account three metrics: the soil storage STO_i; total storage (TS_i) at each simulated day i, which is the sum of soil storage and groundwater storage ($TS_i = STO_i + GW_i$); and the mean total storage TSi, which is the sum of soil storage STOi and temporally-averaged (mean) groundwater storage estimate, over the calibration periods, GW ($TS_i = STO_i + GW$). The latter metric was used because it damps the large uncertainty in GW estimates, and makes the analysis and inter-site differences clearer. This is because the storage in groundwater storage is poorly identified, giving wide variations in the volume of the possible groundwater store at some sites. Despite this, the annual variability in the store is typically small (< 10 mm) so that the effect on the day-to-day catchment storage dynamics is minor as these are mainly dominated by the variation in the soil store, which can vary by > 300 mm. We did not average across the parameter sets on a daily basis because at Dry Creek, the large groundwater store had not stabilized, despite the reasonable flow and isotope simulations. The water stored in the snow pack was not included in these storage metrics as it is only considered to contribute to the catchment storage dynamics once it has melted and infiltrated the soil.

We analysed the temporal storage dynamics of ET and the three storage metrics using raw values (mm or mm/day) and also scaling the time series by mean storage. Scaled values are identified with a *; for instance, the scaled mean total storage is \overline{TS}_i^* is defined as:

$$\bar{TS}_{i}^{*} = \frac{\bar{TS}_{i}}{\mu(\bar{TS})}$$

where μ is the mean and i refers to simulated day.

To analyse Q and Age dynamics, we used the time series of simulated values at the outlet cell of each catchment without further averaging.

Storage, fluxes, and water ages are the system states that we have considered to investigate differences between catchments. The state of the catchment (e.g. its storage) at a given point in time, and the velocity at which such state is changing (time-derivative of the state), were represented by a point in the phase plane spanned by these two variables (Fig. 4). Changes in a catchment over time (i.e. the catchment dynamics) are represented by trajectories in this phase plane. The collection of these trajectories produces an empirical portrait of the dynamic system. Compactness, asymmetry, angles, spikes and seasonal patterns emerging in the portrait can give insights into the hydrology of the catchment function (Sivakumar et al., 2007; Maneta et al., 2018). Specifically, for instance in the case of scaled mean total storage dynamics $(TS^*$ vs $\frac{dTS^*}{dt}$), positive values of the time derivative indicate filling states driven by hydroclimatic forcing and antecedent states of the catchment, are more likely to be stochastic. Conversely, the side of phase-space plot with negative time derivates, shows the catchment efficiency in draining the excess water. In particular, the slope of the negative lower boundary of the cloud of trajectories gives a direct

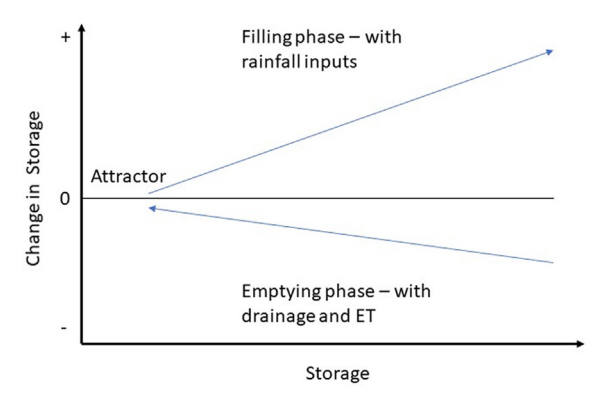


Fig. 4. Conceptual graphic of storage phase-space diagram.

indication of the catchment tendency to quickly release water. Furthermore, the structure of all possible states (compactness or presence of prominent spikes) can give an indication about predominant hydroclimatic conditions or preferential flow generation mechanisms.

3. Results

3.1. Storage dynamics

Box plots of the total storage (TS) in mm show the ranges of sum of soil and groundwater storage, estimated by the STARR model for each of the study sites (Fig. 5). The resulting mean and range have been derived from the simulated storages at each timestep from the five "best" Monte Carlo simulations over the modelled periods (Table 2). Uncertainty in total storage is high, especially at BG and D, mostly due to the high sensitivity of simulated groundwater store to alternative parameterizations. We note that the ranges shown in Fig. 5 account both for the variability in the catchment dynamics as well as the variability of the ensemble induced by the alternative "best" 5 models. The TS is highest in BG (> 2500 mm) and lowest at WC (< 100 mm). Intermediate TS (\sim 500–1000 mm) were modelled for BB and D, whilst TS is also low in KR (\sim 200 mm).

The time series of *STO* (soil storage) and *TS* (mean total storage) are shown for three years of each of the modelled periods (Fig. 6). The catchments have distinct storage dynamics, mainly driven by changes in the soil storage compartment. The uncertainty in upper and lower groundwater contributions to total storage is large, but the upper and

lower limits show the influence of soil store in dominating the overall dynamics. The storage dynamics have a strong hydroclimatic imprint. In BG, STO increases with the spring melt and declines in the summer, before re-wetting with late summer rains prior to remaining stable during the cold winter period. In contrast, at BB STO dynamics are much more variable, generally being highest in the winter, but summer storage depletion is modest and re-filling can occur all year round. The dynamics of D are similar to BB, but a clear spring STO peak occurs after snowmelt, and the potential for depletion (e.g. summer 2012) is much greater. KR is similar to BG in terms of a dominant spring snowmelt event, but also summer peaks from large rainfall events are evident. Changes in STO and TS are small or modest at all sites, with the exception of WC; here STO and TS are lowest in winter as both are impeded by the presence of permafrost, but some storage slowly depletes as some stream flow is maintained. Spring melt increases STO, with storage capacity also increasing with the thaw. However overall changes in STO and TS are very small at WC.

3.2. Phase planes

The scaled mean total storage \overline{TS}^* is plotted against the daily variation of scaled mean total storage $\frac{dTS}{dt}$ in Fig. 7. As suggested, this can be seen as a portrait of the modelled states for each system during the calibration periods (Fig. 7). All sites, apart from WC, show limited variability in TS* due to the high groundwater storage, which produces relatively compact portraits, namely the spread around the $\frac{dTs}{dt} = 0$ line. TS^* increases at BG, BB and D are all < 15% relative to the mean, however at KR it increases by 80%. In contrast, after the prolonged winter period at WC, TS increases by a factor of 5 reflecting non-stationarity in storage capacity in the thaw layer. For the lower storage states, TS^* decreases by < 5% relative to the mean at BG and BB and by < 20% at D and KR. TS^* stays below the mean at WC in winter, early spring and late autumn, as the storage changes little for 8 months. D, KR and WC have the largest variations in TS^* and they can get relatively drier (in terms of their mean storage) than the other catchments. BG has quite small variation in storage despite having similar annual P as KR.

The temporal dynamics shown in Fig. 7 underline the dominant role of soil storage dynamics driving those observed in Fig. 6, with the highest storages in spring for BB, D and KR after snowmelt, though warmer temperatures and rainfall creates the winter peak in BB, and the thaw layer regulates the peak at WC. All sites have lowest storages in

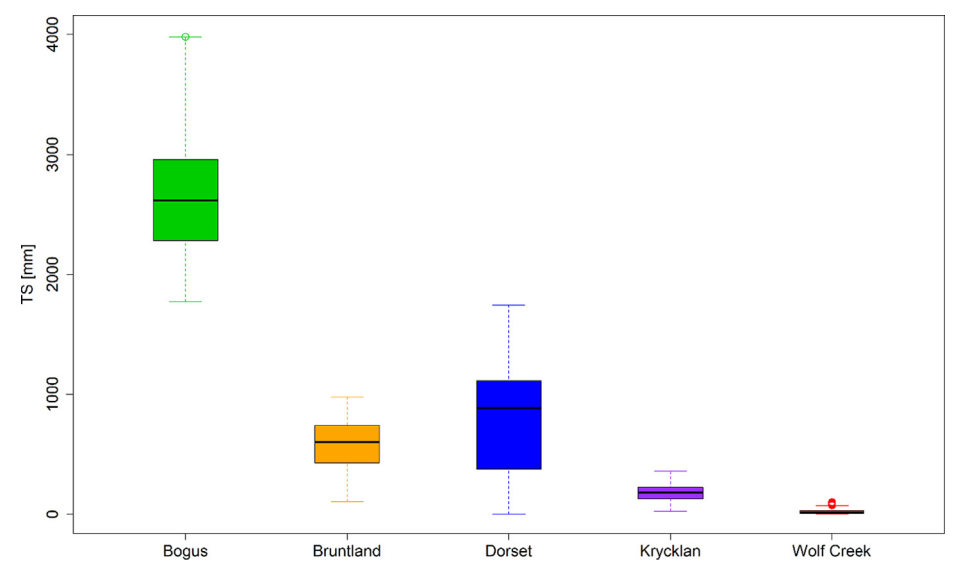


Fig. 5. Boxplot of total storage TS (i.e. soil storage STO + groundwater storage GW), based on the 5 best simulations for each site.

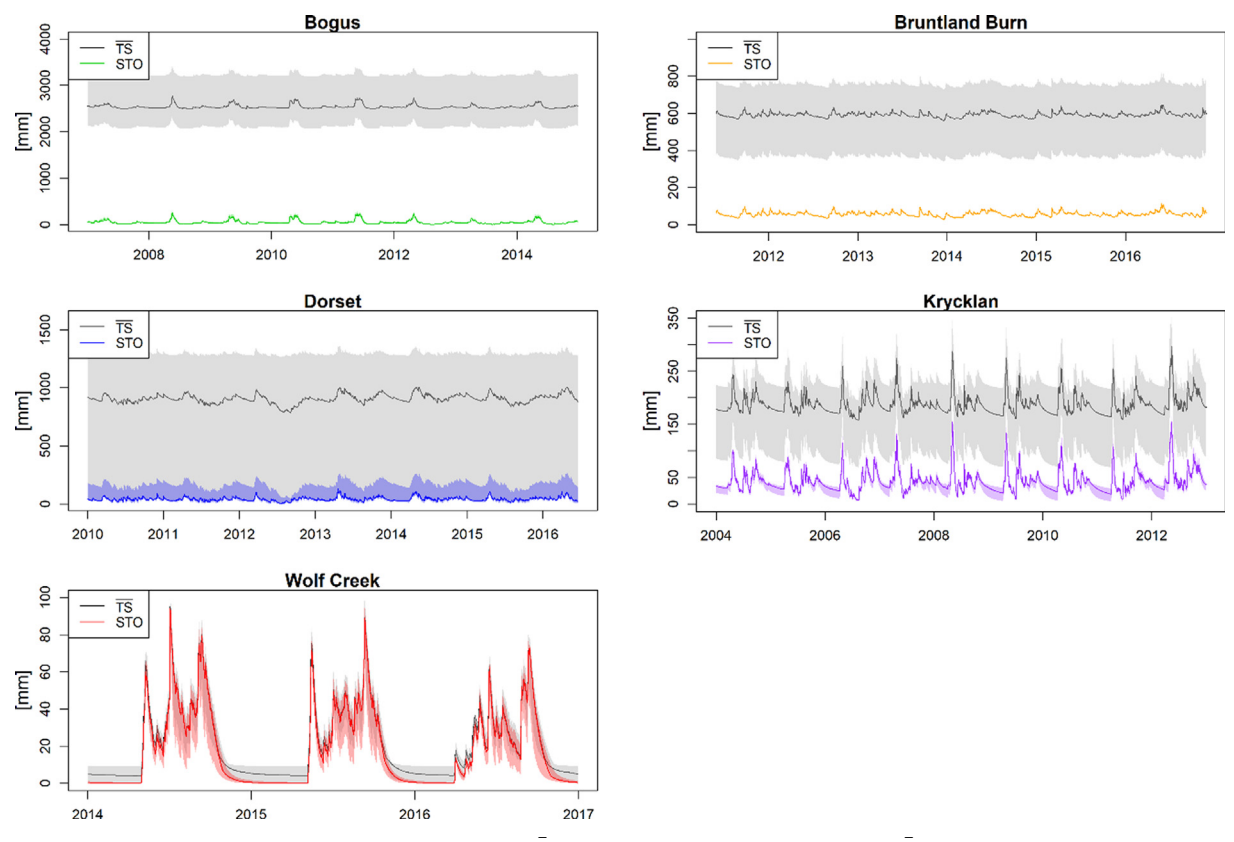


Fig. 6. Time series of simulated soil storage STO and mean total storage TS (soil storage STO + mean groundwater GW). Grey envelopes indicate the uncertainty in 5 best simulations for STO = GW.

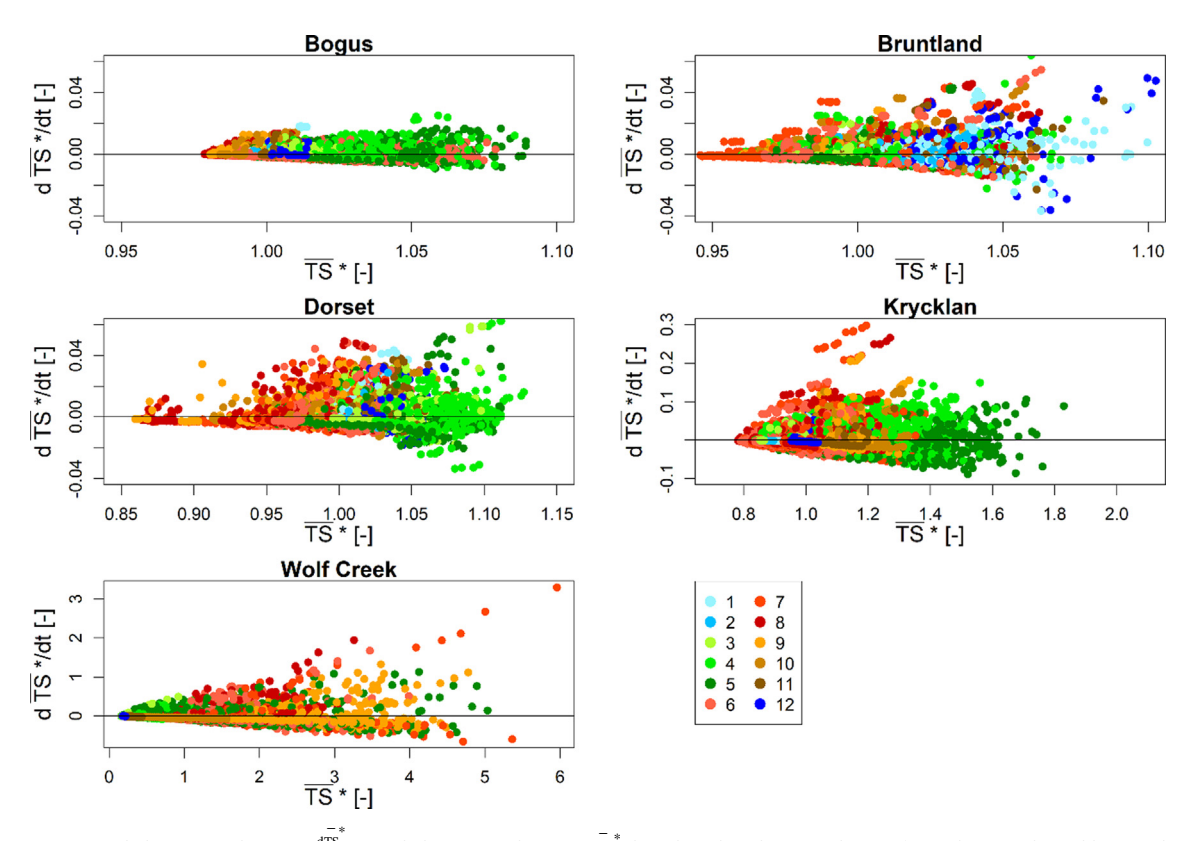


Fig. 7. Daily variation scaled mean total storage $\frac{dTs}{dt}$ vs scaled mean total storage Ts, based on the 5 best simulations for each site, coloured by month (starting with January as "1").

summer, except WC, which is at its driest during winter. The range of the rate of changes of storage $(\frac{dTS}{dt})$ shows only small daily increases of < 2% at BG which are focused in spring whilst increases of < 5% occur at BB, D and KR and can occur at any time of year. Again, at WC much bigger daily increases can occur given the non-linear nature of the storage capacity. This suggests that for most catchments only a very small portion of water is actually flowing in or out of storage at any point in time.

Overall, the most apparent features of these figures reflect the climatic forcing of precipitation or snowmelt during the wetting cycle of the catchment (positive $\frac{dT_s}{dt}$) and catchment characteristics that regulate the rainfall-runoff response and control drainage (negative $\frac{dTs}{dt}$). All catchments are asymmetrical around the $\frac{dT^*}{dt} = 0$ line. Catchment states in the positive $\frac{dT_s}{dT_s}$ section of the plane are driven by the hydroclimatology (rainfall/snowmelt events, seasonality, and the antecedent state of the catchment) and therefore shows higher stochasticity. BG is perhaps an exception: wetting of catchment is mainly driven by a more gradual melt resulting in a more symmetrical diagram and a more orderly configuration in the positive $\frac{d\overline{T^*}}{dt}$ section. Negative $\frac{d\overline{T^*}}{dt}$ responses in the state-space reflect the drainage efficiency of a catchment. The shape of the lower limit of the cloud is mostly driven by the hydrologic processes that drain excess water from the catchment. The line enveloping the lower end of the cloud gently slopes toward the $\frac{dTS}{dt} = 0$ line. The slope of this line is inversely related to the residence time of water and indicates that rate at which excess storage is removed from the catchment.

The non-linearity of catchment functioning is most obvious during high storage states mainly for negative values of TS, most likely when rapid flow paths (e.g. overland flow) are activated and the drainage efficiency increases, especially at BB and D. In particular, inflection points in the bottom boundary slope around TS = 1.04 are evident at BB and D, while they are not apparent at the other sites. There are also differences in the rates at which the catchments fill and empty, i.e. the minimum value of TS resulting in a variation of $\frac{dTS}{dt}$. In D, higher storage is necessary for activating flow paths, except for a few summer events with a faster response. BB storage dynamics also show that it takes a relatively high amount of storage build-up before water starts to drain, while both BG, KR and WC activation of draining mechanisms occur as soon as the catchment gains from its lowest storage.

Differences in the structure (compactness and spikes) of the phase space diagrams are apparent in different seasons within each of the diagrams. Prominent spikes are apparent in periods that are mostly rain-driven (for BB all year; WC and KR in summer; D in spring and summer) which results in less compacts diagrams than catchments that are mostly snowmelt-driven where regular daily energy inputs melt the snow and slowly fill the catchment. Rain storms provide faster rates of filling (high $\frac{dTS}{dt}$) during discrete events producing large spikes in the diagrams compared to snowmelt events, which are reflected in the lower but continuous positive $\frac{dTS}{dt}$. The smooth filling trajectories are most clear in the spring for all catchments except BB. Also, D can have marked rain-on-snow events resulting in spring time high storage increases.

The dynamics of total storage in Fig. 7 primarily reflect soil moisture dynamics, including the influence of the snow melt dynamics. Fig. 8a shows the actual soil storage STO change in mm versus the daily variation of the storage $\frac{dSTO}{dt}$ (i.e. without the mean groundwater storage included). The changes are asymmetrical and greater for the storage increases and more linear on the decreasing side of 0 change. Seasonal pattern in all catchments are similar to Fig. 7, except for D, that here presents high STO and high $\frac{dSTO}{dt}$ during summer, which is

absent in \overline{TS}^* plot (Fig. 7). BG shows more scattered values of $\frac{dSTO}{dt}$ than in the case of \overline{TS}^* plot. Fig. 8b shows the same relationships, but for each ensemble parameter set. In general, the parameter sets give broadly similar results, though the high storage of one parameter set at D reflects the uncertainty in the groundwater storage at this site (cf Fig. 6), and the compensatory effects on soil parameterisation when the former is low.

To explore the role of ET in depleting catchment storage, Fig. 9 shows the pattern of modelled ET against the daily variation of scaled mean total storage $\frac{dTS}{dt}$. The expected relationship would varyin symmetry around the $\frac{dTS}{dt}=0$ depending on the dynamics of storage in relation to evaporative demand. The role of ET in reducing catchment storage is apparent in the figure: although ET can be high both when storage is increasing (particularly notable at BG), the highest ET at most sites tends to be when storage is most slowly decreasing. The effect of ET is evident in D (as expected from the vegetation characteristics and warmer summers) and KR, which presents a similar seasonal response. At BB, there are less distinct seasonal patterns and low rates overall and a smaller influence of ET on storage rates throughout the year. In WC, despite the overall coldest conditions and the predominance of short shrub, a summer influence of ET in storage dynamics is also apparent. BG is the only case where there is a lack of seasonal asymmetry around the $\frac{dTS}{dt}=0$ line, which presumably reflects its dry nature and that moisture is limiting in summer.

3.3. Storage-fluxes and storage-ages dynamics

The relationship between scaled mean total storage \overline{TS}^* and simulated daily discharge Q for each catchment is shown in Fig. 10. All catchments show a non-linear relationship (except for linear relationship at WC), with increased scatter at high TS^* for BB and KR. This would be consistent with the activation of flow pathways such as extensive overland flow, and the development of high hydrologic connectivity within the catchment as storage increases. The higher variance of Q when the catchment is wet also reflects the higher sensitivity of Q to the five different parameters sets in the calibration ensemble when the catchment is at high storage levels. There is a clear non-linear relationship at BG, but the variance of the spread increases when TS increases. At D, streamflow seems less sensitive to storage but shows more scatter when TS^* increases. The relationship is more linear for WC, though is more clearly hysteretic, with higher discharges for a given storage in the spring and with linear response to the thaw and refreeze. However, this likely reflects simply the time-varying storage which increases with the thaw.

To better investigate the possible presence of hysteresis in these storage-discharge relationships, Fig. 11 shows the mean total storage \overline{TS} vs discharge for only one year and for only one of the 5 best simulations. At BG and D, the storage-discharge relationship follows an anticlockwise hysteretic pattern during spring, when higher values of storage and discharge occurred. Hysteresis at BB and KR is much weaker or non-evident. Again, WC showed two hysteretic paths, one in spring and one in summer, due to the different seasonal response and soil parameterisation to allow a thaw layer to developed.

Fig. 12 shows the relationship between scaled mean total storage TS^* and simulated stream water age at the outlet cell. The figure shows the ubiquity of "inverse storage" effects, whereby the wetter the catchment, the more likely it is that younger water reaches the streams more quickly via lateral flow paths. Given that water ages are derived by flux tracking within the model calibrated to the stream isotopes, they should be considered only indicative, especially regarding ages older than a few years. In general, the overall behaviour is similar, with all catchments showing a non-linear decline in the age of streamflow as storage increases. The patterns of seasonality are similar for BG, D and

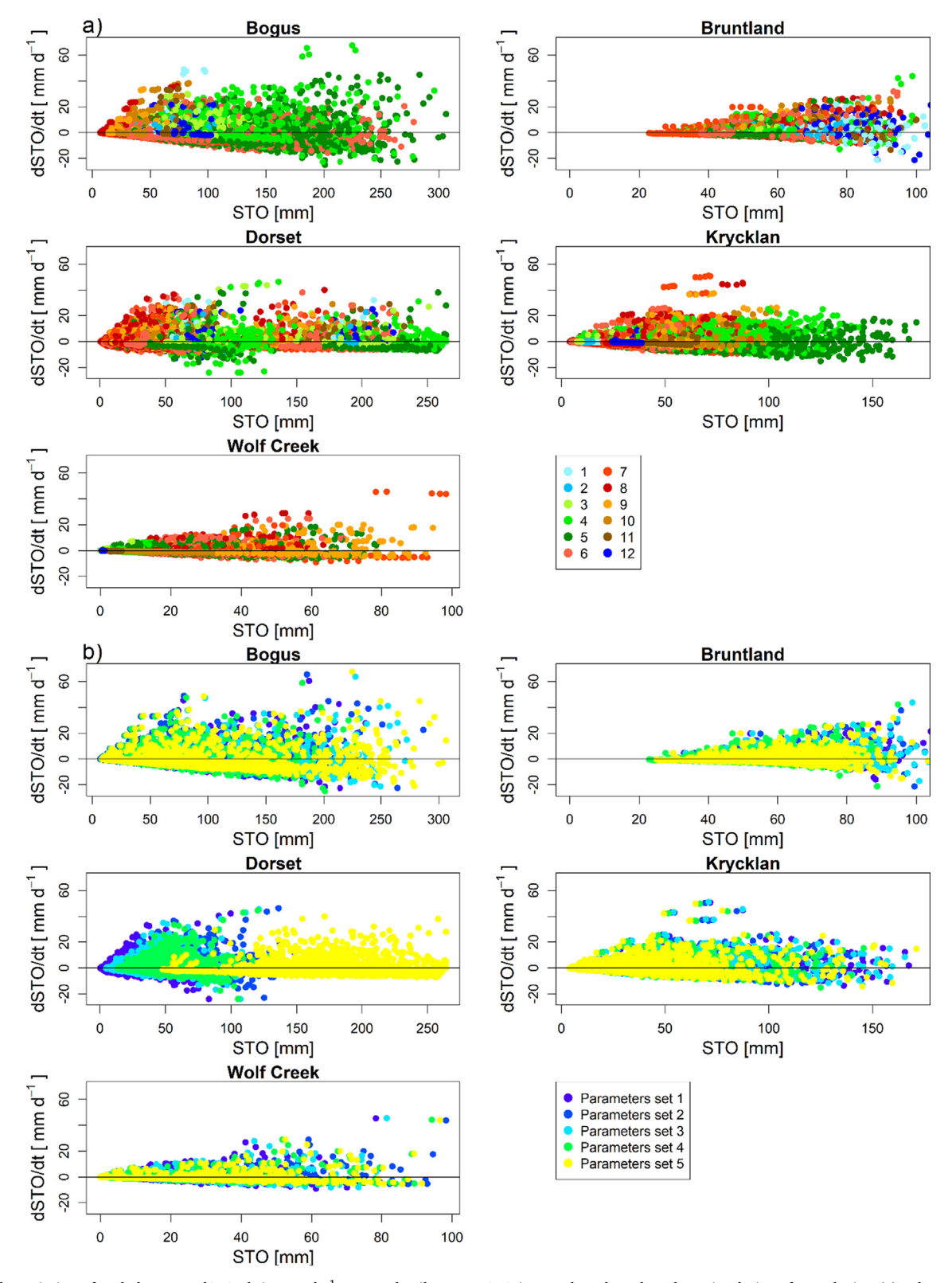


Fig. 8. Daily variation of scaled storage dSTO/dt in mm d^{-1} vs actual soil storage STO in mm, based on the 5 best simulations for each site, (a) coloured by month (starting with January as "1") and (b) according to parameter set.

KR. In these catchments spring snowmelt reduces the age of stream flow as \overline{TS}^* increases. As inputs of younger water decline after the melt, the modelled ages of water in the summer increase, \overline{TS}^* decreases, and groundwater sustains the modelled flow. Different modelled responses are evident at BB as winter rainfall generated higher \overline{TS}^* and low stream

water ages occur. WC, shows a threshold with ages steadily increasing during winter low flows, but rapidly decreasing as thaw occurs. Again, some of the scatter reflects variability induced by uncertainty in the model parametrisation, most obviously in the case of D during the summer.

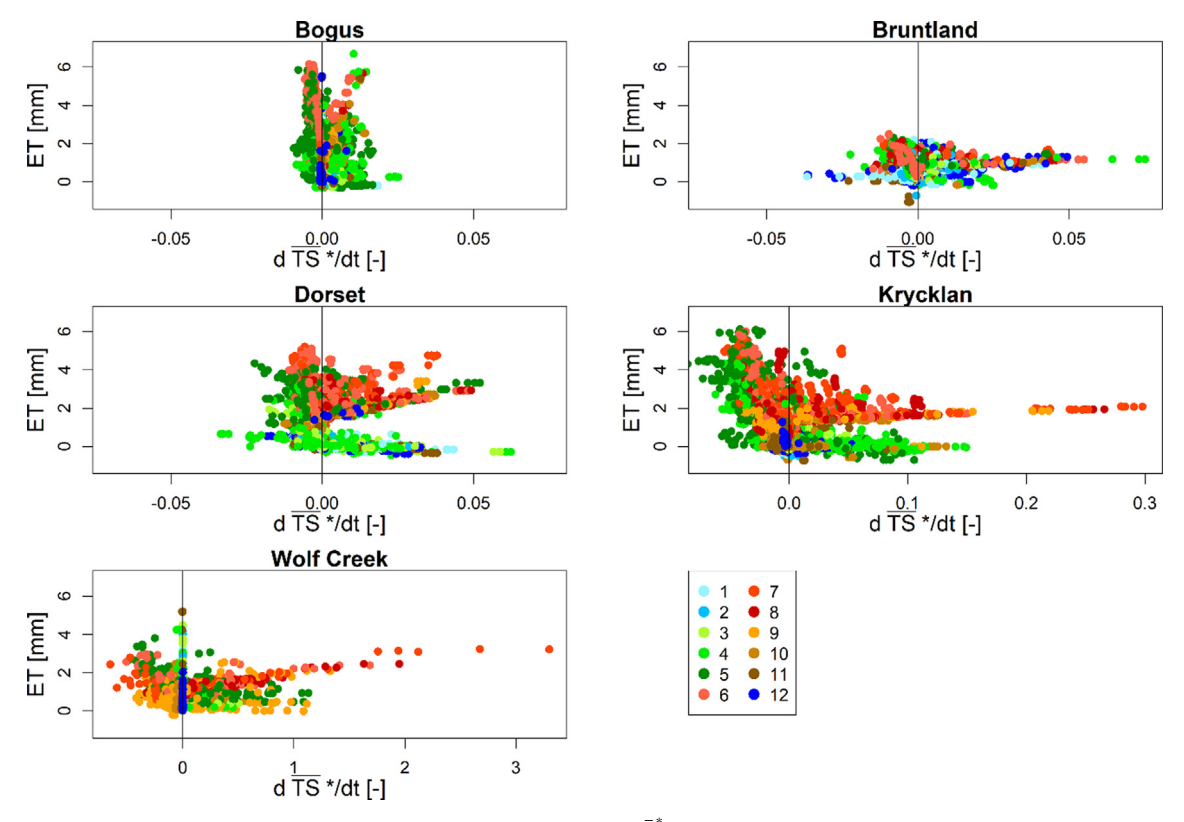


Fig. 9. Simulated evapotranspiration ET vs daily variation of scaled mean total storage $\frac{drs}{dt}$, based on the 5 best simulations for each site, coloured by month (starting with January as "1").

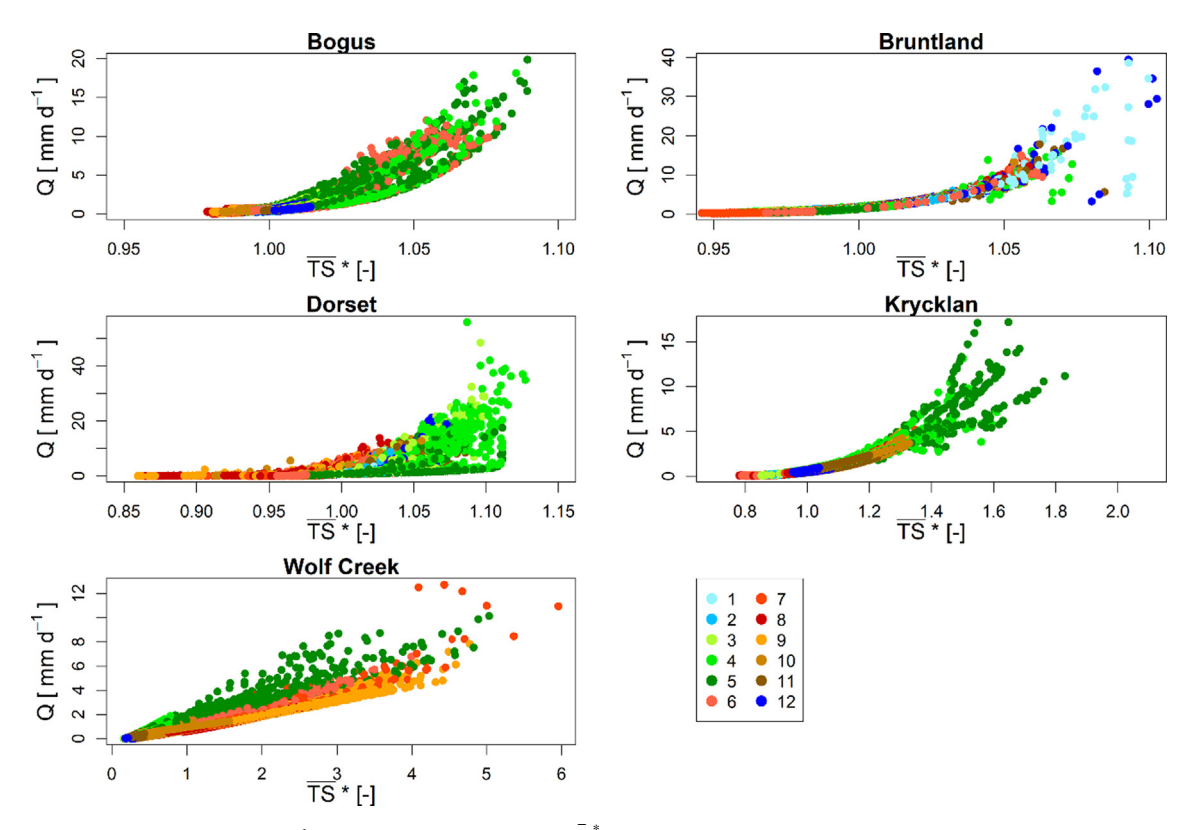


Fig. 10. Simulated daily discharge Q [mm d^{-1}] vs scaled mean total storage TS^* , based on the 5 best simulations for each site, coloured by month (starting with January as "1").

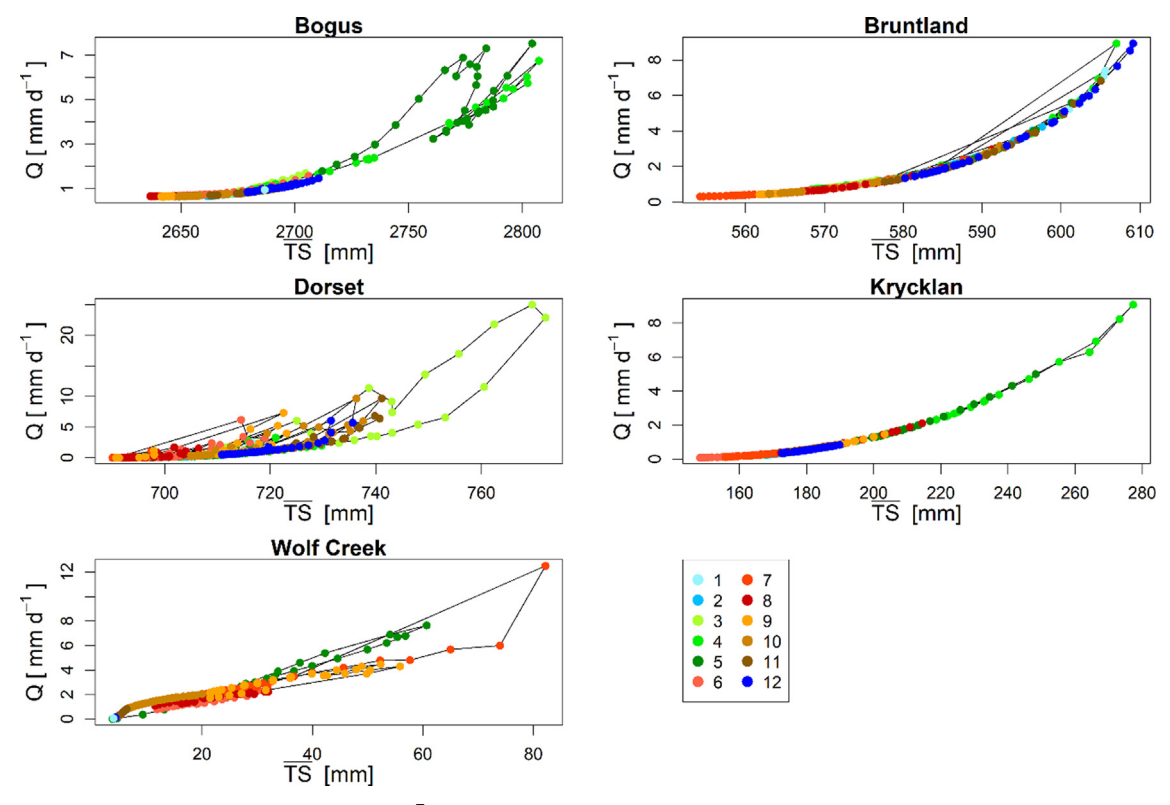


Fig. 11. Simulated daily discharge Q vs mean total storage TS for only one simulated year, coloured by month, in only one of the 5 best simulations in order to investigate the possible presence of hysteresis in the relationship.

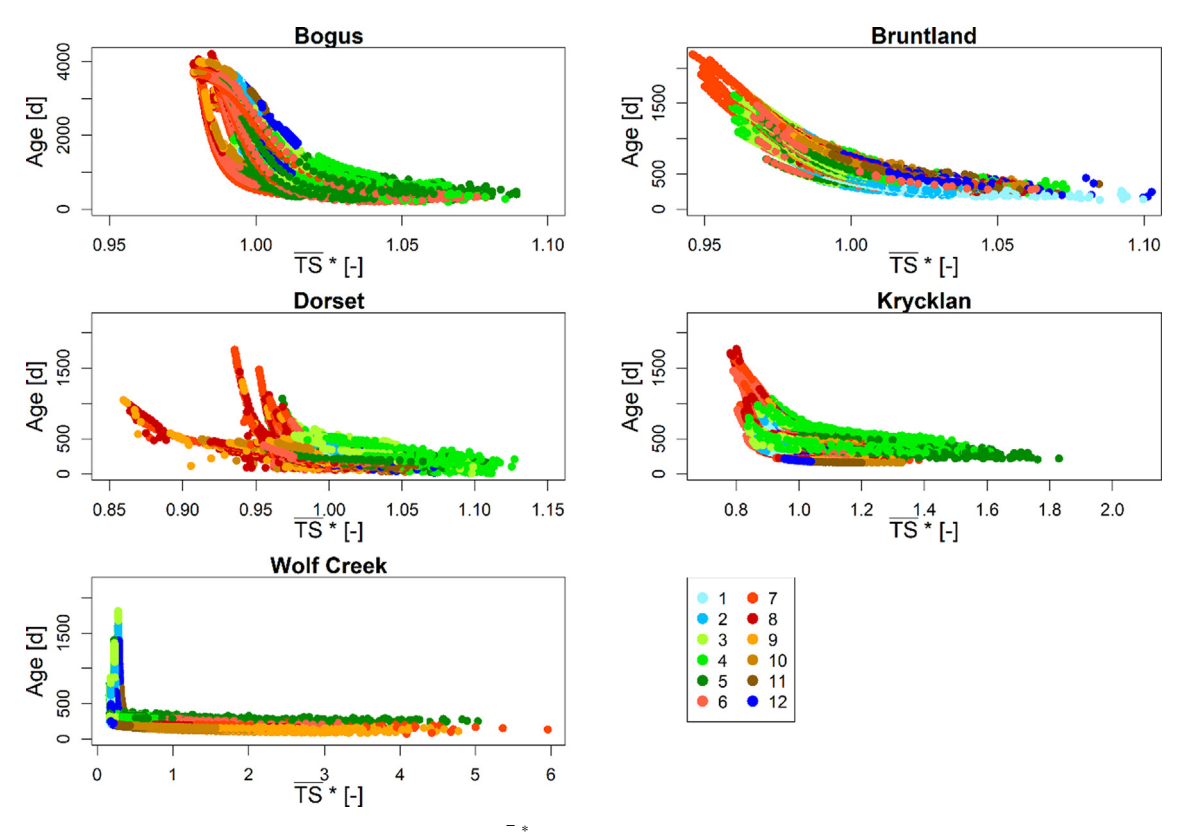


Fig. 12. Simulated stream water age (Age) vs scaled mean total storage TS*, based on the 5 best simulations for each site, coloured by month (starting with January as "1").

Journal of Hydrology 590 (2020) 125226

4. Discussion

4.1. Storage dynamics

McNamara et al. (2011) argued that hydrologists have traditionally focused more on quantifying fluxes than storage in catchment systems, resulting in a distorted view of catchment functioning. Over the past decade, this has changed and different empirical and modelling based approaches have been used to quantify storage and characterise storage dynamics and associated interrelationship with different water fluxes and associated ages (Kirchner, 2009; Heidbüchel et al., 2012; Benettin et al., 2015; Harman, 2015). The use of tracer-aided models has important potential in this regard. Although, such modelling exercises provide storage estimates that are not "real" or "actual" but a simplification, isotopes or other conservative tracers provide important constraints of minimal storage needed to damp and lag the tracer inputoutput transformation (Kirchner et al., 2000). Crucially, this usually shows that such storages are at least an order of magnitude larger than dynamic storage changes needed to close the annual water balance (Staudinger et al., 2017). Consequently, this provides a more comprehensive understanding of the filling and emptying of storage in catchments in response to snowmelt and rainfall events, as well as insight into the associated age distributions of both stores and fluxes.

In the context of the current study, such modelled storage provides a useful set of metrics for inter-comparison of catchment behaviour and sensitivity to change (e.g. Figs. 5 and 6) that is not possible from more conventional rainfall-runoff modelling. Also, given the rich observational data sets at each of the sites, the plausibility of the modelling results can be assessed. For example, the high total storage TS and long age distributions at BG are consistent with the geological conditions and high levels of mountain block groundwater recharge in the area (McNamara et al., 2018). Similarly, the critical role of snowmelt in governing soil water replenishment of plant water transpirations sources, ground recharge and stream flow responses has been documented (McNamara et al., 2005; Sprenger et al., 2018a). At BB, previous work has shown how saturated valley bottom wetlands rapidly respond to precipitation events, but damp tracer signals because of their large near-surface storage capacity in STO (Soulsby et al., 2015). The generally wet summers and low radiation in the Scottish Highlands limit evapotranspiration fluxes and gravity drainage in the steep catchment dominates the dynamic storage responses to precipitation inputs (Tetzlaff et al., 2014). However, the effects of high groundwater storage in deeper drift deposits were also captured by the model in terms of sustaining the quantify and isotopic composition of baseflows (Soulsby et al., 2016). D and KR show similarities in their storage dynamics due to the dominance of the spring snowmelt in re-filling storage, but also the effects of summer rainfall events. However, at KR, a relatively low storage is inferred as near-surface hydrological processes in perennially wet organic soils dominate storm runoff generation (Peralta-Tapia et al., 2015a). Thus, both runoff responses and isotope damping can be adequately captured with relatively low volumes of active storage (Laudon et al., 2007). In D, however, most parameter sets infer that a significant large store is needed to do the same (Buttle, 1994); though as Figs. 6 and 8b show, it is uncertain whether this is mainly in the soils or groundwater. This result is consistent with the presence of the conifer-dominated wetland and the role that exerts on catchment streamflow response (Devito et al., 1996). The wetland acts as an additional store when the water table has been drawn down and thus no streamflow response is recorded, while in case of summer rainfall events on wet wetland area generates flow peaks. In WC, the extensive presence of permafrost means that storage is largely regulated by the development of a thaw layers in the organic soils as the summer evolves (McCartney et al., 2006). This mediates the translation of snowmelt into runoff as well as the impact of late summer rainfall (Quinton et al., 2004; Dornes et al., 2008). Of course, at WC the permafrost is also a water "store", though one that does not actively

contribute runoff when frozen, though thaw layers are likely to penetrate deeper and active greater volumes of such storage in the future as the climate warms (Piovano et al., 2019).

Overall, the value of such storage-based catchment inter-comparison is that it highlights the role of both hydroclimatic drivers and catchment characteristics in determining the sensitivity of storage dynamics (Beven and Davies, 2015). This, in turn, can provide insight into the likely resilience of storage to climate and other environmental change (Carey et al., 2010). In this regard, the likely reduced influence of the snowpack as climatic warming advances, will shift the runoff regime at these sites, which might increase winter runoff from rainfall and reduce storage at the start of the growing season, which is currently dependably supplied by spring snowmelt.

4.2. Storage phase changes

The reconstruction of the phase portraits for each catchment provides a framework for catchment inter-comparison by showing the unique filling and emptying trajectories that reflect responses to climate inputs and internal function. Apart from WC, the scaled plots in Fig. 7 highlight just how small the dynamic storage changes are relative to the total active storage estimated from the STARR applications. The critical role of the wet organic soils at all sites apart from BG in modulating these phases changes is apparent from Fig. 8a. The positive change in storage section of the plot in Fig. 7 show the stochastic effect of rainfall events in the data spread at B, D and KR, whilst much more systematic melt effects at BG and WC produce a more compact plot. On the other hand, the negative change in storage section of the plot, which represents the drying of the catchment, is more predictable. The drying is dominated by gravity drainage when the catchments are in wetter conditions, although the role of ET is also important at some of the sites as conditions become drier (Fig. 9). In the wettest conditions, sites like BB. D and WC the drying trajectories in the phase space show distinct non-linearity, presumably because hydrological connectivity is greatest during wet conditions and rapid flow paths can drain the catchment more effectively in the initial stages of drying. The uncertainty in the phase space plots is indicated for the soil storage in Fig. 8b. Although this is similar for most sites, D - which has the greatest groundwater uncertainty (Fig. 6) - has some variation reflecting the compensatory effect of calibration producing a larger groundwater store/smaller soil water store or, in the case of parameter set 5, vice versa.

4.3. Storage-Fluxes and Storage-Ages dynamics

The non-linear storage-discharge relationships for the catchments generally show more scatter at higher storages (see example year in Fig. 11). In part this reflects the non-linearity of the catchment function and the higher sensitivity in responses of catchments when they are wet (Harman, 2015), but also highlights that model outputs can be more sensitive to parameterization errors when at high storage (Fig. 8b). The non-stationary, but more linear, relationship at WC reflects the shifting storage capacity as thaw develops and then ends. The modelled storage-discharge relationship shows anticlockwise hysteresis at BG and D, showing storage replenishment, while the relationships for BB and KR lack hysteresis. At WC, some hysteresis is evident in larger, late summer rainfall where some storage has developed in the thaw layer.

Interestingly, the modelled results support the inverse storage effect at multiple sites, in that higher storages result in younger streamflow. This is consistent with increased lateral water movement in the surface and near-surface and transport of younger water into the streams (Harman, 2015). All sites show that baseflows are a few years old, whilst in the wettest conditions water ages are typically < 1 year old. The sites show similarities, especially BB and KR, whilst BG is an outlier in terms of the much older baseflows associated with the large storage and relatively low fluxes. WC is also unique in terms of the binary switch when the thaw layer develops in summer. Meanwhile D shows

T. Piovano, et al. Journal of Hydrology 590 (2020) 125226

the effect of a wide spread of modelled results, mostly in summer. This underlines the utility of tracer-aided modelling in terms of providing plausible characterisation of storage dynamics that can then provide age estimates of stream flow. This more comprehensive perspective on the catchment rainfall-runoff response that reconciles both the response celerity and velocity of water particles provides a much firmer evidence base for assessing the likely implications of both climate and land use change (e.g. Smith et al., 2020).

5. Conclusion

We used the spatially distributed, tracer-aided STARR model to examine the storage dynamics of contrasting long-term research catchments in northern latitudes. This enabled us to understand storage controls on the magnitude, seasonality and age of stream water fluxes. Multi-calibration of models on both hydrometric and stream isotope data revealed that total storage in all catchments was much greater than the dynamic storage inferred by water balance considerations. Phase space diagrams were found to be useful tools to observe and compare distinctive features of storage dynamics. Clear in the diagrams were the nature of water inputs (rainfall and/or snowmelt), and how the internal catchment drainage mechanisms and ET demands regulated storage dynamics in each catchment. The results demonstrated that the storagedischarge relationships are increasingly non-linear as catchments become wetter, and rainfall - rather than snowmelt - forms the dominant input. Furthermore, we found that hydrological connectivity increases surface and near-surface runoff processes during wetter conditions, but these processes often cease rapidly after inputs stop. This explains the ubiquity of the "inverse storage effect" whereby conditions of higher storage selectively move younger water to streams. The study highlights the potential benefits of cautious use of multi-calibrated tracer-aided models to understand storage-flux-age interactions in northern catchments, which in turn influences their sensitivity to environmental change.

CRediT authorship contribution statement

T. Piovano: Conceptualization, Formal analysis, Visualization, Software, Writing - original draft. D. Tetzlaff: Supervision, Project administration, Funding acquisition, Writing - review & editing. M. Maneta: Conceptualization, Methodology, Writing - review & editing. J.M. Buttle: Investigation, Writing - review & editing. S.K. Carey: Investigation, Writing - review & editing. H. Laudon: Investigation, Writing - review & editing. J. McNamara: Investigation, Writing - review & editing. C. Soulsby: Conceptualization, Methodology, Supervision, Writing - review & editing.

Declaration of Competing Interest

The authors declare that they have no known competing financial interests or personal relationships that could have appeared to influence the work reported in this paper.

Acknowledgments

This work was funded by the European Research Council (project GA 335910 VeWa). Funding for maintaining KR comes from Swedish Science Foundation (SITES), Formas, SKB, SLU and KAW (Branch-Points).

References

Ala-aho, P., Tetzlaff, D., McNamara, J.P., Laudon, H., Kormos, P., Soulsby, C., 2017a. Modeling the isotopic evolution of snowpack and snowmelt: Testing a spatially distributed parsimonious approach. Water Resour. Res. 53, 5813–5830. https://doi.org/10.1002/2017WR020650. Ala-aho, P., Tetzlaff, D., McNamara, J.P., Laudon, H., Soulsby, C., 2017b. Using isotopes to constrain water flux and age estimates in snow-influenced catchments using the STARR (Spatially distributed Tracer-Aided Rainfall-Runoff) model. Hydrol. Earth Syst. Sci. 21, 5089–5110. https://doi.org/10.5194/hess-21-5089-2017.

- Benettin, P., Bailey, S.W., Campbell, J.L., Green, M.B., Rinaldo, A., Likens, G.E., McGuire, K.J., Botter, G., 2015. Linking water age and solute dynamics in streamflow at the Hubbard Brook Experimental Forest, NH, USA. Water Resour. Res. 51, 9256–9272. https://doi.org/10.1002/2015WR017552.
- Beven, K., Davies, J., 2015. Velocities, celerities and the basin of attraction in catchment response. Hydrol. Process. 29, 5214–5226. https://doi.org/10.1002/hyp.10699.
- Beven, K.J., 1993. Prophecy, reality and uncertainty in distributed hydrological modelling. Adv. Water Resour. 16, 41–51.
- Birkel, C., Geris, J., Molina, M.J., Mendez, C., Arce, R., Dick, J., Tetzlaff, D., Soulsby, C., 2016. Hydroclimatic controls on non-stationary stream water ages in humid tropical catchments. J. Hydrol. 542, 231–240. https://doi.org/10.1016/j.jhydrol.2016.09.
- Birkel, C., Soulsby, C., 2015. Advancing tracer-aided rainfall-runoff modelling: a review of progress, problems and unrealised potential. Hydrol. Process. 29, 5227–5240. https://doi.org/10.1002/hyp.10594.
- Birkel, C., Soulsby, C., Tetzlaff, D., 2015. Conceptual modelling to assess how the interplay of hydrological connectivity, catchment storage and tracer dynamics controls nonstationary water age estimates. Hydrol. Process. 29, 2956–2969. https://doi.org/ 10.1002/hyp.10414.
- Birkel, C., Soulsby, C., Tetzlaff, D., 2011. Modelling catchment-scale water storage dynamics: reconciling dynamic storage with tracer-inferred passive storage. Hydrol. Process. 25, 3924–3936. https://doi.org/10.1002/hyp.8201.
- Brandes, D., Duffy, C.J., Cusumano, J.P., 1998. Stability and damping in a dynamical model of hillslope hydrology. Water Resour. Res. 34, 3303–3313.
- Buttle, J.M., 1994. Isotope hydrograph separations and rapid delivery of pre-event water from drainage basins. Prog. Phys. Geogr. 18, 16–41. https://doi.org/10.1177/ 030913339401800102.
- Carey, S.K., Tetzlaff, D., Seibert, J., Soulsby, C., Buttle, J., Laudon, H., McDonnell, J., McGuire, K., Caissie, D., Shanley, J., Kennedy, M., Devito, K., Pomeroy, J.W., 2010. Inter-comparison of hydro-climatic regimes across northern catchments: synchronicity, resistance and resilience. Hydrol. Process. 24, 3591–3602. https://doi.org/10.1002/hyp.7880.
- Dehaspe, J., Birkel, C., Tetzlaff, D., Sanchez-Murillo, R., Duran-Quesada, A.M., Soulsby, C., 2018. Spatially-distributed tracer-aided modelling to explore water and isotope transport, storage and mixing in a pristine, humid tropical catchment. Hydrol. Process. 32, 3206–3224. https://doi.org/10.1002/hyp.13258.
- Delavau, C.J., Stadnyk, T., Holmes, T., 2017. Examining the impacts of precipitation isotope input (δ18O ppt) on distributed, tracer-aided hydrological modelling. Hydrol. Earth Syst. Sci. 21, 2595–2614. https://doi.org/10.5194/hess-21-2595-2017.
- Devito, K.J., Hill, A.R., Roulet, N., 1996. Groundwater-surface water interactions in headwater forested wetlands of the Canadian Shield. J. Hydrol. 181, 127–147. https://doi.org/10.1016/0022-1694(95)02912-5.
- Dillon, P.J., LaZerte, B.D., 1992. Response of the Plastic Lake catchment, Ontario, to reduced sulphur deposition. Environ. Pollut. 77, 211–217. https://doi.org/10.1016/ 0269-7491(92)90079-P.
- Dooge, J.C.I., 1967. A new approach to nonlinear problems in surface water hydrology: hydrologic systems with uniform nonlinearity. Int. Assoc. Sci. Hydrol. Publ. 76,
- Dornes, P.F., Pomeroy, J.W., Pietroniro, A., Carey, S.K., Quinton, W.L., 2008. Influence of landscape aggregation in modelling snow-cover ablation and snowmelt runoff in a sub-arctic mountainous environment. Hydrol. Sci. J. 53, 725–740. https://doi.org/ 10.1623/hysj.53.4.725.
- Douinot, A., Tetzlaff, D., Maneta, M., Kuppel, S., Schulte-Bisping, H., Soulsby, C., 2019. Ecohydrological modelling with EcH2O-iso to quantify forest and grassland effects on water partitioning and flux ages. Hydrol. Process. 33, 2174–2191. https://doi.org/ 10.1002/hyp.13480.
- Duffy, C.J., 1996. A two-state integral-balance model for soil moisture and groundwater dynamics in complex terrain. Water Resour. Res. 32, 2421–2434.
- Dunn, S., Bacon, R., J.,, 2008. Assessing the value of Cl and δ 18O data in modelling the hydrological behaviour of a small upland catchment in northeast Scotland. Hydrol. Res. 39, 337–358. https://doi.org/10.2166/nh.2008.134.
- Fenicia, F., McDonnell, J.J., Savenije, H.H.G., 2008a. Learning from model improvement: On the contribution of complementary data to process understanding. Water Resour. Res. 44, 1–13. https://doi.org/10.1029/2007WR006386.
- Fenicia, F., Savenije, H.H.G., Matgen, P., Pfister, L., 2008b. Understanding catchment behavior through stepwise model concept improvement. Water Resour. Res. 44, 1–13. https://doi.org/10.1029/2006WR005563.
- Georgakakos, K.P., Sharifi, M.B., Sturdevant, P.L., 1995. Analysis of high-resolution rainfall data, in: Kundzewicz, Z.W. (Ed.), New Uncertainty Concepts in Hydrology and Water Resources. Cambridge University Press, Cambridge, pp. 114–120. https:// doi.org/10.1017/CBO9780511564482.012.
- Gupta, H.V., Kling, H., Yilmaz, K.K., Martinez, G.F., 2009. Decomposition of the mean squared error and NSE performance criteria: implications for improving hydrological modelling. J. Hydrol. 377, 80–91. https://doi.org/10.1016/j.jhydrol.2009.08.003.
- Harman, C.J., 2015. Time-variable transit time distributions and transport: theory and application to storage-dependent transport of chloride in a watershed. Water Resour. Res. 51, 1–30. https://doi.org/10.1002/2014WR015707.
- Heidbüchel, I., Troch, P.A., Lyon, S.W., Weiler, M., 2012. The master transit time distribution of variable flow systems. Water Resour. Res. 48, 1–19. https://doi.org/10.1029/2011WR011293.
- Houghton, J., 1991. The Bakerian Lecture, 1991. The predictability of weather and climate. Philos. Trans. Phys. Sci. Eng. 337, 521–572.

T. Piovano, et al. Journal of Hydrology 590 (2020) 125226

Hrachowitz, M., Savenije, H., Bogaard, T.A., Tetzlaff, D., Soulsby, C., 2013. What can flux tracking teach us about water age distribution patterns and their temporal dynamics? Hydrol. Earth Syst. Sci. 17, 533–564. https://doi.org/10.5194/hess-17-533-2013.

- Hrachowitz, M., Soulsby, C., Tetzlaff, D., Malcolm, I.A., Schoups, G., 2010. Gamma distribution models for transit time estimation in catchments: physical interpretation of parameters and implications for time-variant transit time assessment. Water Resour. Res. 46. https://doi.org/10.1029/2010WR009148.
- Iorgulescu, I., Beven, K.J., Musy, A., 2005. Data-based modelling of runoff and chemical tracer concentrations in the Haute-Mentue research catchment (Switzerland). Hydrol. Process. 19, 2557–2573. https://doi.org/10.1002/hyp.5731.
- Jayawardena, A.W., Lai, F., 1994. Analysis and prediction of chaos in rainfall and stream flow time series. J. Hydrol. 153, 23–52.
- Kirchner, J.W., 2009. Catchments as simple dynamical systems: catchment characterization, rainfall-runoff modeling, and doing hydrology backward. Water Resour. Res. 45, 1–34. https://doi.org/10.1029/2008WR006912.
- Kirchner, J.W., 2006. Getting the right answers for the right reasons: linking measurements, analyses, and models to advance the science of hydrology. Water Resour. Res. 42, 1–5. https://doi.org/10.1029/2005WR004362.
- Kirchner, J.W., 2003. A double paradox in catchment hydrology and geochemistry. Hydrol. Process. 17, 871–874. https://doi.org/10.1002/hyp.5108.
- Kirchner, J.W., Feng, X., Neal, C., 2000. Fractal stream chemistry and its implications for contaminant transport in catchments. Nature 403, 524–527. https://doi.org/10. 1038/35000537
- Kirkwood, D.E., Nesbitt, H.W., 1991. Formation and evolution of soils from an acidified watershed: Plastic Lake, Ontario, Canada. Geochim. Cosmochim. Acta 55, 1295–1308. https://doi.org/10.1016/0016-7037(91)90308-R.
- Koutsoyiannis, D., Pachakis, D., 1996. Deterministic chaos versus stochasticity in analysis and modeling of point rainfall series. J. Geophys. Res. 101, 441–451.
- Kuppel, S., Tetzlaff, D., Maneta, M.P., Soulsby, C., 2018. What can we learn from multi-data calibration of a process-based ecohydrological model? Environ. Model. Softw. 101, 301–316. https://doi.org/10.1016/j.envsoft.2018.01.001.
- Laudon, H., Löfvenius, M.O., 2016. Adding snow to the picture providing complementary winter precipitation data to the Krycklan Catchment Study database. Hydrol. Process. 30, 2413–2416. https://doi.org/10.1002/hyp.10753.
- Laudon, H., Mo, M., Buffam, I., Seibert, J., Sjo, V., 2007. The role of catchment scale and landscape characteristics for runoff generation of boreal streams. J. Hydrol. 344, 198–209. https://doi.org/10.1016/j.jhydrol.2007.07.010.
- Laudon, H., Taberman, I., Ágren, A., Futter, M., Ottosson-löfvenius, M., Bishop, K., 2013. The Krycklan Catchment Study — a flagship infrastructure for hydrology, biogeochemistry, and climate research in the boreal landscape. Water Resour. Res. 49, 7154–7158. https://doi.org/10.1002/wrcr.20520.
- Lindström, G., Johansson, B., Persson, M., Gardelin, M., Bergström, S., 1997.
 Development and test of the distributed HBV-96 hydrological model. J. Hydrol. 201, 272–288. https://doi.org/10.1016/S0022-1694(97)00041-3.
- Lorenz, E.N., 1991. Dimension of weather and climate attractors. Nature 353, 241–244. https://doi.org/10.1038/353241a0.
- Maneta, M.P., Soulsby, C., Kuppel, S., Tetzlaff, D., 2018. Conceptualizing catchment storage dynamics and nonlinearities. Hydrol. Process. 32, 3299–3303. https://doi. org/10.1002/hyp.13262.
- McCartney, S.E., Carey, S.K., Pomeroy, J.W., 2006. Intra-basin variability of snowmelt water balance calculations in a subarctic catchment. Hydrol. Process. 20, 1001–1016. https://doi.org/10.1002/hyp.6125.
- McDonnell, J.J., Beven, K., 2014. Debates—The future of hydrological sciences: a (common) path forward? A call to action aimed at understanding velocities, celerities and residence time distributions of the headwater hydrograph. Water Resour. Res. 50, 5342–5350. https://doi.org/10.1002/2013WR015141.
- McNamara, J.P., Benner, S.G., Poulos, M.J., Pierce, J.L., Chandler, D.G., Kormos, P.R., Marshall, H.-P., Flores, A.N., Seyfried, M., Glenn, N.F., Aishlin, P., 2018. Form and function relationships revealed by long-term research in a semiarid mountain catchment. Wiley Interdiscip. Rev. Water 5, e1267. https://doi.org/10.1002/wat2.1267
- McNamara, J.P., Chandler, D., Seyfried, M., Achet, S., 2005. Soil moisture states, lateral flow, and streamflow generation in a semi-arid, snowmelt-driven catchment. Hydrol. Process. 19, 4023–4038. https://doi.org/10.1002/hyp.5869.
- McNamara, J.P., Tetzlaff, D., Bishop, K., Soulsby, C., Seyfried, M., Peters, N.E., Aulenbach, B.T., Hooper, R., 2011. Storage as a metric of catchment comparison. Hydrol. Process. 25, 3364–3371. https://doi.org/10.1002/hyp.8113.
- Peralta-Tapia, A., Soulsby, C., Tetzlaff, D., Sponseller, R., Bishop, K., Laudon, H., 2016. Hydroclimatic influences on non-stationary transit time distributions in a boreal headwater catchment. J. Hydrol. 543, 7–16. https://doi.org/10.1016/j.jhydrol.2016. 01.079.
- Peralta-Tapia, A., Sponseller, R.A., Ågren, A., Tetzlaff, D., Soulsby, C., Laudon, H., 2015a. Scale-dependent groundwater contributions influence patterns of winter baseflow stream chemistry in boreal catchments. J. Geophys. Res. Biogeosci. 120, 847–858. https://doi.org/10.1002/2014JG002878.
- Peralta-Tapia, A., Sponseller, R.A., Tetzlaff, D., Soulsby, C., Laudon, H., 2015b. Connecting precipitation inputs and soil flow pathways to stream water in contrasting boreal catchments. Hydrol. Process. 29, 3546–3555. https://doi.org/10.1002/hyp. 10300.
- Piovano, T.I., Tetzlaff, D., Ala-aho, P., Buttle, J., Mitchell, C.P.J., Soulsby, C., 2018. Testing a spatially distributed tracer-aided runoff model in a snow-influenced catchment: effects of multicriteria calibration on streamwater ages. Hydrol. Process. 32, 3089–3107. https://doi.org/10.1002/hyp.13238.
- Piovano, T.I., Tetzlaff, D., Carey, S.K., Shatilla, N.J., Smith, A., Soulsby, C., 2019. Spatially distributed tracer-aided runoff modelling and dynamics of storage and water ages in a permafrost-influenced catchment. Hydrol. Earth Syst. Sci. 23,

- 2507-2523. https://doi.org/10.5194/hess-23-2507-2019.
- Porporato, A., Ridolfi, L., 2003. Detecting determinism and nonlinearity in river-flow time series. Hydrol. Sci. J. 48, 763–780. https://doi.org/10.1623/hysj.48.5.763. 51457
- Puente, C.E., Obregn, N., 1996. A deterministic geometric representation of temporal rainfall. Results for a storm in Boston. Water Resour. Res. 32, 2825–2839.
- Quinton, W.L., Carey, S.K., Goeller, N.T., 2004. Snowmelt runoff from northern alpine tundra hillslopes: major processes and methods of simulation. Hydrol. Earth Syst. Sci. 8, 877–890. https://doi.org/10.5194/hess-8-877-2004.
- Rinaldo, A., Beven, K.J., Bertuzzo, E., Nicotina, L., Davies, J., Fiori, A., Russo, D., Botter, G., 2011. Catchment travel time distributions and water flow in soils. Water Resour. Res. 47, 1–13. https://doi.org/10.1029/2011WR010478.
- Robinson, J.S., Sivapalan, M., Snell, J.D., 1995. On the relative roles of hillslope processes, channel routing, and network geomorphology in the hydrologic response of natural catchments. Water Resour. Res. 31, 3089–3101.
- Rodell, M., Velicogna, I., Famiglietti, J.S., 2009. Satellite-based estimates of groundwater depletion in India. Nature 460, 999–1002. https://doi.org/10.1038/nature08238.
- Rodriguez-Iturbe, I., De Power, B.F., 1989. Chaos in rainfall. Water Resour. Res. 25, 1667–1675.
- Sharifi, M.B., Georgakakos, K.P., Rodriguez-Iturbe, I., 1990. Evidence of deterministic chaos in the pulse of storm rainfall. J. Atmos. Sci. 47, 888–893.
- Sivakumar, B., 2000. Chaos theory in hydrology: important issues and interpretations. J. Hydrol. 227, 1–20.
- Sivakumar, B., Berndtsson, R., Olsson, J., Jinno, K., Olsson, J., Jinno, K., 2009. Evidence of chaos in the rainfall-runoff process. Hydrol. Sci. J. 46, 131–145. https://doi.org/ 10.1080/02626660109492805.
- Sivakumar, B., Jayawardena, A.W., Li, W.K., 2007. Hydrologic complexity and classification: a simple data. Hydrol. Process. 21, 2713–2728. https://doi.org/10.1002/hyp.
- Sivakumar, B., Liong, S.-Y., Liaw, C.-Y., Phoon, K.-K., 1999. Singapore rainfall behaviour: chaotic? J. Hydrol. Eng. 4, 38–48.
- Sivakumar, B., Singh, V.P., 2012. Hydrologic system complexity and nonlinear dynamic concepts for a catchment classification framework. Hydrol. Earth Syst. Sci. 16, 4119–4131. https://doi.org/10.5194/hess-16-4119-2012.
- Smith, A.A., Tetzlaff, D., Laudon, H., Maneta, M., Soulsby, C., 2019. Assessing the influence of soil freeze-thaw cycles on catchment water storage flux age interactions using a tracer-aided ecohydrological model. Hydrol. Earth Syst. Sci. Discuss.
- Smith, A.A., Tetzlaff, D., Kleine, L., Maneta, M., Soulsby, C., 2020. Isotope-aided modelling of ecohydrologic fluxes and water ages under mixed land use in central Europe: the 2018 drought and its recovery. Hydrol. Process. https://doi.org/10.1002/hyp. 13838
- Soulsby, C., Birkel, C., Geris, J., Dick, J., Tunaley, C., Tetzlaff, D., 2015. Stream water age distributions controlled by storage dynamics and nonlinear hydrologic connectivity: modeling with high-resolution isotope data. Water Resour. Res. 51, 7759–7776. https://doi.org/10.1002/2015WR017888.
- Soulsby, C., Bradford, J., Dick, J., Mcnamara, J.P., Geris, J., Lessels, J., 2016. Using geophysical surveys to test tracer-based storage estimates in headwater catchments. Hydrol. Process. 30, 4434–4445. https://doi.org/10.1002/hyp.10889.
- Soulsby, C., Piegat, K., Seibert, J., Tetzlaff, D., 2011. Catchment-scale estimates of flow path partitioning and water storage based on transit time and runoff modelling. Hydrol. Process. 25, 3960–3976. https://doi.org/10.1002/hyp.8324.
- Sprenger, M., Tetzlaff, D., Buttle, J., Carey, S.K., McNamara, J.P., Laudon, H., Shatilla, N.J., Soulsby, C., 2018a. Storage, mixing, and fluxes of water in the critical zone across northern environments inferred by stable isotopes of soil water. Hydrol. Process. 32, 1720–1737. https://doi.org/10.1002/hyp.13135.
- Sprenger, M., Tetzlaff, D., Buttle, J., Laudon, H., Soulsby, C., 2018b. Water ages in the critical zone of long-term experimental sites in northern latitudes. Hydrol. Earth Syst. Sci. 22, 3965–3981. https://doi.org/10.5194/hess-22-3965-2018.
- Stadnyk, T., Amour, N.S.T., Kouwen, N., Edwards, T.W.D., Pietroniro, A., 2005. A groundwater separation study in boreal wetland terrain: the WATFLOOD hydrological model compared with stable isotope tracers. Isot. Env. Heal. Stud. 41, 49–68. https://doi.org/10.1080/10256010500053730.
- Stadnyk, T.A., Delavau, C., Kouwen, N., Edwards, T.W.D., 2013. Towards hydrological model calibration and validation: simulation of stable water isotopes using the isoWATFLOOD model. Hydrol. Process. 27, 3791–3810. https://doi.org/10.1002/ hyp. 9695
- Staudinger, M., Stahl, K., Stoelzle, M., Seeger, S., Seibert, J., Weiler, M., 2017. Catchment water storage variation with elevation. Hydrol. Process. 31, 2000–2015. https://doi. org/10.1002/hyp.11158.
- Tetzlaff, D., Birkel, C., Dick, J., Geris, J., Soulsby, C., 2014. Storage dynamics in hydropedological units control hillslope connectivity, runoff generation, and the evolution of catchment transit time distributions. Water Resour. Res. 50, 969–985. https://doi.org/10.1002/2013WR014147.
- Tetzlaff, D., Buttle, J., Carey, S.K., Huijgevoort, M.H.J. Van, Laudon, H., Mcnamara, J.P., Mitchell, C.P.J., Spence, C., Gabor, R.S., Soulsby, C., 2015a. A preliminary assessment of water partitioning and ecohydrological coupling in northern headwaters using stable isotopes and conceptual runoff models. Hydrol. Process. 29, 5153–5173. https://doi.org/10.1002/hyp.10515.
- Tetzlaff, D., Buttle, J., Carey, S.K., Mcguire, K., Laudon, H., Soulsby, C., 2015b. Tracerbased assessment of flow paths, storage and runoff generation in northern catchments: a review. Hydrol. Process. 29, 3475–3490. https://doi.org/10.1002/hyp. 10412.
- Tsonis, A.A., Elsner, J.B., Georgakakos, K.P., 1993. Estimating the dimension of weather and climate attractors: important issues about the procedure and interpretation. J. Atmos. Sci. 50, 2549–2555.
- Uhlenbrook, S., Roser, S., Tilch, N., 2004. Hydrological process representation at the

- meso-scale: the potential of a distributed, conceptual catchment model. J. Hydrol.
- 291, 278–296. https://doi.org/10.1016/j.jhydrol.2003.12.038. van Huijgevoort, M.H.J., Tetzlaff, D., Sutanudjaja, E.H., Soulsby, C., 2016a. Using high resolution tracer data to constrain water storage, flux and age estimates in a spatially distributed rainfall-runoff model. Hydrol. Process. 30, 4761-4778. https://doi.org/ 10.1002/hyp.10902.
- van Huijgevoort, M.H.J., Tetzlaff, D., Sutanudjaja, E.H., Soulsby, C., 2016b. Visualization of spatial patterns of connectivity and runoff ages derived from a tracer-aided model.
- Hydrol. Process. 30, 4893-4895. https://doi.org/10.1002/hyp.10961.
- Weiler, M., McGlynn, B.L., McGuire, K.J., McDonnell, J.J., 2003. How does rainfall become runoff? A combined tracer and runoff transfer function approach. Water Resour. Res. 39, 1-13. https://doi.org/10.1029/2003WR002331.
- Zhang, Z., Chen, X., Cheng, Q., Soulsby, C., 2019. Storage dynamics, hydrological connectivity and flux ages in a karst catchment: conceptual modelling using stable isotopes. Hydrol. Earth Syst. Sci. 23, 51-71. https://doi.org/10.5194/hess-23-51-2019.